

VOLUME 14 ISSUE 2

LIDAR

SPRING 2024

MAGAZINE



MONTICELLO REVEALED

16 3D AI IN THE HIGH-DENSITY PROCESS

How artificial intelligence has improved point-cloud classification at IGN, France's national mapping agency

22 DIGITAL TWIN OPENS RAINFOREST

Advanced geospatial technology is being used to map one of nature's most complex creations—the tropical rainforest

33 SURFACE WATER AND DRAINAGE

Accurate data for surface water and drainage proves crucial for planning, engineering and daily operations



Frontier Precision has the latest LiDAR, Photogrammetry, & Remote Dock innovations to fit your job or application.

Our staff has the knowledge and real-world experience to help you select the solution that's best for you and the training to make you more proficient and profitable.



AUTONOMOUS DATA COLLECTION FROM ANYWHERE.



DJI DOCK



Skydio



YellowScan

The YellowScan LiDAR UAV delivers the highest level of accuracy and density for real-time georeferenced point cloud data.



emesent

Emesent automates the collection and analysis of data in challenging GPS-denied environments, delivering revolutionary efficiency, safety, and operational insights for the industry.



INSPIRED FLIGHT

dji ENTERPRISE

WATTS INNOVATIONS

CENSYS TECHNOLOGIES

AUTEL ROBOTICS



Parrot

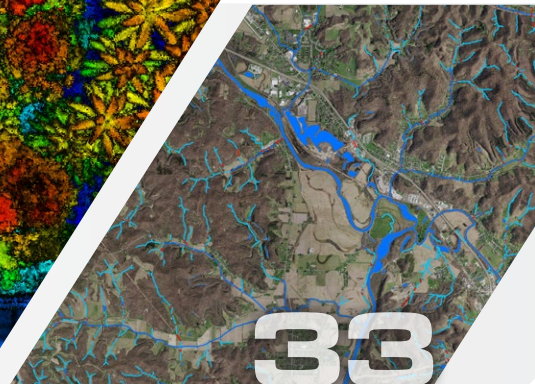
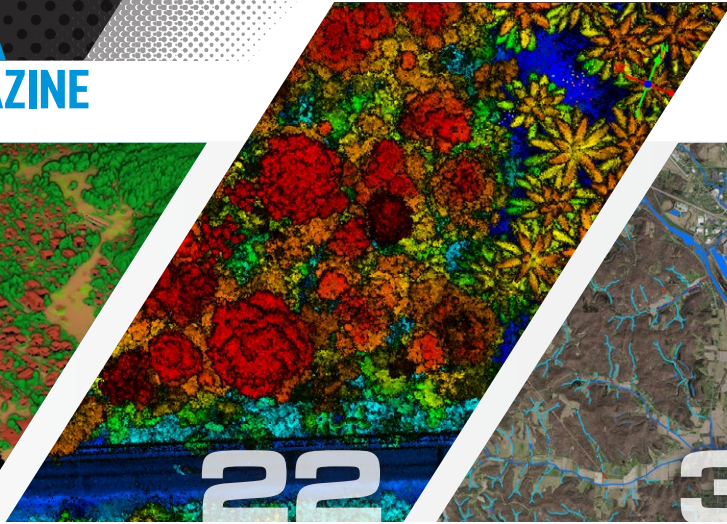
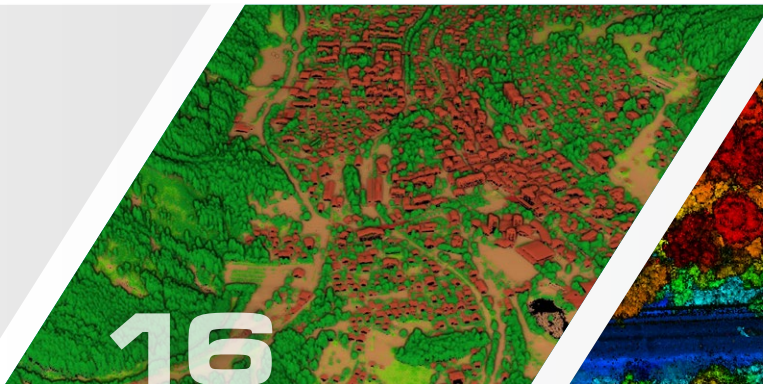
FREEFLY

**FRONTIER PRECISION | CORPORATE
FOR MORE INFORMATION CALL 701.222.2030 OR 800.359.3703**



LIDAR

MAGAZINE



IN THIS ISSUE

8 Lidar Brings Monticello Into Focus

One of the most important sources of new discoveries is the Monticello Plantation Archaeological Survey, an ongoing effort to locate all the archaeological sites and traces of past land use on the 2500 acres currently owned by the Thomas Jefferson Foundation, the non-profit responsible for Monticello's preservation and interpretation.

BY: BRAD BARKER AND DEREK WHEELER

16 3D AI in the Lidar HD Production Process

Designed to meet the needs of various public actions (flood risk prevention, estimation of forest resources, etc.), the Lidar HD program aims to provide a 3D description of the French territory by 2025. Operated by the French Mapping Agency, the project is funded by governmental allocations and regional authorities' support.

BY FLORYNE ROCHE

22 Digital Twins Open Up Rainforest Conservation

Imagine a digital twin. Perhaps you are imagining the digital representation of a chip inside a phone or of a manufacturing shop floor, or even an entire digitized city. Now imagine using this capability for a rainforest in Costa Rica where jaguars roam and exotic birds perch in ancient and medicinal trees.

BY ANDREW KERR

26 Continuous Flow Surface Hydrography Feature Extraction

Over the past 20 years, lidar-derived digital elevation models (DEMs) have become the staple of surface-water hydrography and hydraulic (H&H) modeling. During this same period, lidar has evolved significantly in terms of both absolute three-dimensional (horizontal and vertical) spatial accuracy. Most recently, two distinct lidar technologies have emerged, linear-mode and Geiger-mode.

BY AL KARLIN

33 Decades of Historic Data Finished

Accurate geospatial data on surface water and drainage is crucial for planning, engineering, and daily operational activities for every county in every state. Nevertheless, Ohio has coped for decades without a full set of timely, comprehensive geospatial surface water and drainage data. This shortfall has prevented stakeholders from understanding current drainage scenarios.

BY BRIAN STEVENS

37 Evaluating Accuracy according to the New ASPRS Standards

This article was inspired by a comment I received: "Even after 24 years as a land surveyor, I can still use refreshing on how to explain the basics to my clients and surveyors-in-training. Your in-depth discussion on the difference between the standard deviation and the root mean square error (RMSE) was very appreciated."

BY QASSIM ABDULLAH

COLUMNS

4 From the Editor: A Digital Record

BY DR. STEWART WALKER

48 Full Coverage: The quest for "wall-to-wall" coverage for hydrosatial applications

BY AMAR NAYEGANDHI (& AL KARLIN)

LIDAR To Go!

Get the most from this magazine on your tablet or laptop.



◀ ON THE COVER

Sunrise over Thomas Jefferson's Monticello, Charlottesville, Virginia. Image courtesy of the Thomas Jefferson Foundation, a non-profit responsible for the historic plantation's preservation and interpretation. Achieving the Plantation Survey's goals requires accurate maps, and the accuracy of the maps available to the Foundation's archaeologists has radically improved thanks to aerial lidar.

SCAN
PROCESS
MODEL
OFFER
WIN
MORE



DISCOVER
NAVVIS
VLX 3

navvis.com/lsp

Cloud computing and software have rapidly changed the world around us in fundamental ways. But not all industries can move at the same pace. Our cities, homes, schools, bridges, roads, and offices are all still built using the same core principles that date back millennia: reliable and precise measurements. Why? Because they work. When it comes to understanding the world around us, when laying the foundations of our economies, infrastructure, and systems, **reliability and precision are essential.**

While our principles stay the same, the world around us continues to change, to grow, and to speed up. Architecture, engineering, and construction projects are more ambitious, their scope and scale continuing to grow with every year. Public investment in infrastructure projects is rising but time frames for completion are getting shorter, all while regulatory and safety requirements are more stringent and exacting. **Our principles stay the same, but our methods have to evolve** to keep us fit for purpose.

New methods and tools need to integrate with and evolve existing toolkits and practices. Drawing on the established power of software and the cloud, **NavVis helps Laser Scanning Professionals expand** their scanning, processing, and modeling toolkit **in a natural, necessary way.**

The principles of reliability and precision are unchanged.

NavVis helps you do more with them – quickly documenting, verifying, and collaborating on the world around us. NavVis gives Laser Scanning Professionals the right tools for the job so they can scan, process and model more data, from more sites, for more clients – **in less time.**



A Digital Record

Our cover story is about an archaeological application. Well-known geospatial services company Surdex¹ was contracted by the Thomas Jefferson Foundation to acquire lidar of the Jefferson plantation in Monticello, Virginia. Not surprisingly, the new data has engendered many discoveries that were simply not possible with previous techniques. We've become accustomed to staggering discoveries through lidar's penetration of vegetation, but it's worth remembering that this need not be in tropical rainforest—the advantages bear fruit in temperate climes too. The authors mention the Cahokia site near St. Louis—there is a plethora of literature on this, including a useful, short piece on some surveying aspects². I cite this as a reminder that there's a lot more to archaeological surveys in the 21st century than photogrammetry and lidar: the Cahokia piece described a geophysical survey of the site, just as our Monticello piece concludes that the lidar data facilitates decision-making on the most promising places to conduct sediment analyses using a range of the latest techniques.

We are fortunate to share an article by Qassim Abdullah that is also running in *Photogrammetric Engineering & Remote Sensing*. This focuses on an aspect of Edition 2 of the *ASPRS Positional Accuracy Standards for Digital Geospatial Data* and emphasizes a self-evident truth: the ground control points and independent check points that we use to georeference then QC lidar surveys are themselves not perfect but are subject to errors, i.e. their coordinates in whatever datum is being used are not error-free and this has to be taken into account when estimating and publishing the accuracy of the lidar. Sometimes it's hard to put numbers on the accuracy of the survey of the control and check points, but Qassim gives guidelines and typical values that can be used.

Crossing the Atlantic, we are pleased to offer an engaging article by Floryne Roche of the French national mapping agency, IGN, on the use of artificial intelligence to help with the processing of lidar data. France is heavily engaged on a nationwide lidar program, called HD Lidar, with similarities to the USGS 3DEP program, so the requirement for reliable, automated techniques to facilitate the massive data-processing task is an urgent one. IGN's approach is both leading-edge and practical.

Contributing writer Al Karlin has provided yet another significant article. Lidar is being used all over the world to extract hydrographic and hydrologic features—stream geometries, hierarchies and so on. Al has looked at data sets of parts of Pinellas Country, Florida, to

1 Now part of Bowman Consulting Group: businesswire.com/news/home/20240402970569/en/Bowman-Enters-into-Definitive-Agreement-to-Acquire-Surdex-Corporation-Adding-High-Altitude-Digital-Imagery-Digital-Mapping-and-Advanced-Geospatial-Services

2 Thoresen, J., 2023. The Cahokia mounds, *xyHt*, 10(4): 10-14, April 2023.

LIDAR MAGAZINE

www.lidarmag.com

2024 Vol. 14 No. 2
© Spatial Media LLC

PUBLISHER Allen E. Cheves
publisher@spatialmedia.us

MANAGING EDITOR Dr. A. Stewart Walker
stewart.walker@lidarmag.com

ASSOCIATE PUBLISHER Kevin Grapes
kevin.grapes@spatialmedia.us

EDITOR EMERITUS Marc S. Cheves, LS
marc.cheves@spatialmedia.us

CONTRIBUTING WRITERS

Dr. Qassim Abdullah
Dr. Srinidharan Dharmapuri
Jeff Fagerman
Dr. Juan Fernandez-Diaz
Jason C. Fries
Dr. Al Karlin
Antero Kukko
Aaron Lawrence
Dr. David Maune
Amar Nayegandhi
Mike Shillenn
Evon Silvia
Ken Smerz
Dr. Jason Stoker
Larry Trojak
James Wilder Young
Dr. Michael Zanetti

The staff and contributing writers may be reached via the online message center at our website.

GRAPHIC DESIGN LTD Creative, LLC
WEBMASTER Joel Cheves
AUDIENCE DEVELOPMENT Edward Duff

LIDAR Magazine is published 6x annually by Spatial Media LLC. Editorial mailing address: 7820 B Wormans Mill Road, #236 Frederick, MD 21701. Tel: (301) 620-0784; Fax: (301) 695-1538. No part of this publication may be reproduced in any form without the express written permission of the publisher. Opinions and statements made by the writers and contributors do not necessarily express the views of Spatial Media LLC.

Made in the United States of America

OFFICIAL PUBLICATION





High-Performance INS Solutions for Surveying Applications

NEW QUANTA SERIES

- » Designed for Seamless OEM Integration
- » Robust to Vibrating Environments
- » Post-processing with Qinertia PPK Software



Quanta Micro



Quanta Plus



Quanta Extra



lead.me/lidarmag



see how the results from QL1 and QL2 linear-mode lidar collections and a Geiger-mode collection compare. This is extremely valuable as it gives an idea of what it is reasonable to expect from the different modalities and sensors.

Brian Stevens's piece describes the use of 3DEP and 3DHP by Woolpert to create the Ohio Surface Water Model, a new approach to elevation-derived hydrography. The testimonials from county engineers are heartfelt and encouraging.

Al Karlin has also played a role in the latest installment of Amar Nayegandhi's "Full Coverage" column. These two experts argue the pros and cons of including total propagated uncertainty as lidar metadata. We should reflect on this as LAS, LAZ and other standards advance.

We end with a return to the rainforest—in Costa Rica! Andrew Kerr, from Hexagon's R-evolution—crudely, the green part of the conglomerate—has been working on reforestation using tremendously informative forest data formed by merging airborne lidar from a Leica CountryMapper with ground-based lidar from the handheld BLK2GO. The images in this article are arresting in their intricacy and beauty.

You can learn more about Leica CountryMapper, both its capabilities and the intriguing history behind it, in one of our podcasts. *The LIDAR Magazine Podcasts* are growing as new episodes are added every couple of weeks³. Each is interesting in its own way, but the conversation with Ron Roth of Leica Geosystems, whom I've known for more than 25 years, is poignant.

I like to close editorials with snippets from something I've read. The National Trust is a UK non-profit that protects and

manages coastline, woodlands, countryside and hundreds of historic buildings, gardens and precious collections, many of which were donated by families no longer able to maintain them. Reading a short article in the organization's journal about an initiative to rejuvenate chalk grassland in the South Downs, part of southern England⁴, I learned that the Trust is working with Historic England on mapping the area's many ancient monuments using aerial photography and lidar. Meanwhile, matters are more urgent in Scotland. At Knowe of Swandro, on the island of Rousay, which is in the Orkney archipelago to the north of the Scottish mainland, there are remains of important Iron Age and Norse settlements. Sadly, the sediments on which they are located are being washed away by rising sea level and more frequent storms, both occasioned by climate change⁵. The solution—use lidar and imagery to create a digital record for future generations, just in case the race against the elements is lost.

Reading and editing authors' manuscripts and the resulting proofs is enjoyable yet challenging. But sometimes, while buried in docs/pdfs, one's mind wanders. Almost two years ago, I became treasurer of the International Society for Photogrammetry and Remote Sensing (ISPRS⁶) at its XXIV Congress in Nice, France. I traveled west, on the fast TGV railroad, to Montpellier, to attend the YellowScan "LiDAR for Drone 2022" event. I reported this for readers⁷ and continued by train to Austria, for a morning in beautiful Graz at the facility of Vexcel Imaging. At that time, we knew

Vexcel Imaging as a supplier of top-notch aerial cameras for crewed aircraft, but times have changed. Last year, Vexcel Imaging announced a new product, UltraCam Dragon 4.1, which is based on an integration of its UltraCam Osprey camera with RIEGL's VQ-680 OEM lidar module⁸. Thus this firm is now fully in the lidar world—as opposed to supplying its big cameras to fly in the same aircraft as other suppliers' lidar sensors—so I'm writing up the visit for an article to be published later this year.

I continued eastwards and spent one of the most perfect days of my professional life. Thanks to Johannes Riegl, Jr., of RIEGL USA in Winter Park, Florida, where I attended the opening of the new facility⁹, the folks at RIEGL's headquarters in Horn, north of Vienna, rolled out the red carpet and gave me a day of intense, high-quality presentations intertwined with tours of the various buildings on the campus, and the new instrument test range, where I was honored to have Dr. Andreas Ullrich to accompany me!

I'm currently writing up travels that have taken place since Geo Week in Denver in February 2024—look out for them on the website soon. I believe it's time, as one shivers in the winter of one's career, to thank the people who helped me fashion my career, the magazine for supporting me, the conference organizers, and the magazine's customers for their warm welcomes and unselfish sharing of technologies and ideas. Thanks for the memories.



A. Stewart Walker // Managing Editor

³ lidarmag.com/podcast/

⁴ Beer, H., 2023. Changing Chalk, *National Trust Magazine*, 160: 32-27, autumn 2023.

⁵ Anon, 2024. In ruins: climate change is unearthing and erasing history all at once, *The Economist*, 450(9386): 74, 16 March 2024.

⁶ isprs.org

⁷ lidarmag.com/2022/06/24/nice-is-nice/

⁸ vexcel-imaging.com/the-new-ultracam-dragon-4-1-game-changing-hybrid-oblique-imaging-and-lidar-system/

⁹ lidarmag.com/2021/11/24/riegl-ribbon-cutting



Wingtra LIDAR is now supported by LP360!

The latest updates in LP360 can take your data to the next level.

Are you using the new Wingtra LIDAR Solution to capture 3D data for large aerial surveying projects? Then take that data to the next level with LP360 Drone LiDAR & photogrammetry 3D point cloud software.

With LP360 Drone you can process, analyze, and maximize your Wingtra LiDAR survey data, creating enhanced and highly accurate deliverables.

The fully integrated workflow of LP360 Drone lets you Fly, Optimize and Deliver fully processed data into actionable results. Learn how you can get the most out of your Wingtra LiDAR with LP360 Drone.

Get the most out of your Wingtra LiDAR Data with LP360 Drone

- Manage your coordinate system (geoid, grid to ground, local site, datum and epoch change)
- Leverage LP360 powerful 3 synchronized viewing windows and Image Explorer tool
- QC/QA your data with Automatic Ground Control Detection and 3D Correction
- Access all the other advanced tools such as Smoothing, Automated Outlier Removal, Automatic Classification, Break lines, DTM and Contour Generations, export to CAD formats, volumetric calculations, powerlines encroachment tools and much more
- Customize / define your own workflow with the new GUI
- Go further with unique LP360 Cloud Extension (optional add-on) to store, search, share and stream your data with any LP360 Desktop



Scan to learn more >

SPECIAL OFFER!

Get LP360 Cloud to Make Your Geospatial Work Easier

RIGHT NOW, for any LP360 order, get **3 months of FREE access** to LP360 Cloud and Cloud Starter

LP360 Cloud is an ever-growing collection of cloud-based tools and resources that will make it easy for you to manage, archive, share and collaborate on geospatial projects.

LP360 Cloud is an ever-growing collection of cloud-based tools and resources that will make it easy for you to manage, archive, share and collaborate on geospatial projects.

- Store and manage data
- Stream pointclouds
- Discover Powersearch to localize all available datasets within a geographical area



PODCAST

Listen to additional discussion
at lidarmag.com/podcast



Lidar Brings Monticello into Focus

Thomas Jefferson Foundation commends
discoveries from laser scanning

Today, Thomas Jefferson's Monticello ranks as one of the most important historical sites in the United States. Two centuries ago, Monticello was a 5000-acre plantation that was home not just to Jefferson, but also to hundreds of enslaved people and their families, producing tobacco and later wheat for sale on Atlantic markets. The ongoing interdisciplinary study of the Monticello landscape, the artifacts that lie under it, and surviving documents are providing 21st century Americans with a much clearer

understanding of the property and the lives of all its residents than we had a decade ago.

One of the most important sources of new discoveries is the Monticello Plantation Archaeological Survey, an ongoing effort to locate all the archaeological sites and traces of past land use on the 2500 acres currently owned by the Thomas Jefferson Foundation, the non-profit responsible for Monticello's preservation and interpretation. Achieving the Plantation Survey's goals requires accurate maps, and the

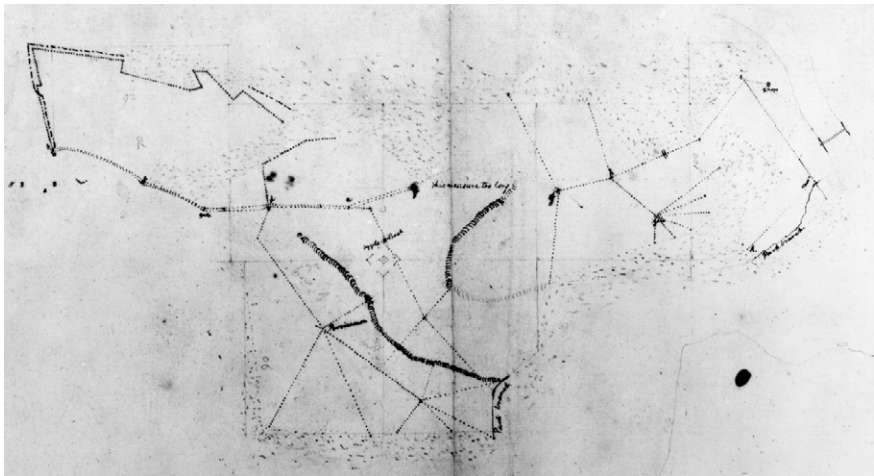
accuracy of the maps available to the Foundation's archaeologists has radically improved thanks to aerial lidar, which has the ability to reveal geographic detail that is otherwise undetectable. Lidar is proving to be a valuable tool in the modern archaeologist's toolbox for uncovering secrets of the past.

Derek Wheeler, Research Archaeologist at the Thomas Jefferson Foundation, relates his reaction to seeing the features revealed by lidar data: "The level of detail that the lidar data provides is astounding—it's like waking

BY BRAD **BARKER** AND DEREK **WHEELER**



Thomas Jefferson's Monticello at sunrise.



Early hand-drawn documents of Monticello Mountain agricultural fields (c. 1795).

up in the morning and putting on my glasses. The world goes from fuzzy and indistinct to clear!”

Brad Barker, Director of 3D Mapping at Surdex, agreed about the increase in detail. “After walking the property of Monticello, I was amazed at the features that could be seen in the lidar. It is easy

to forget the ruggedness of the natural landscape while viewing digital elevation models in the office!”

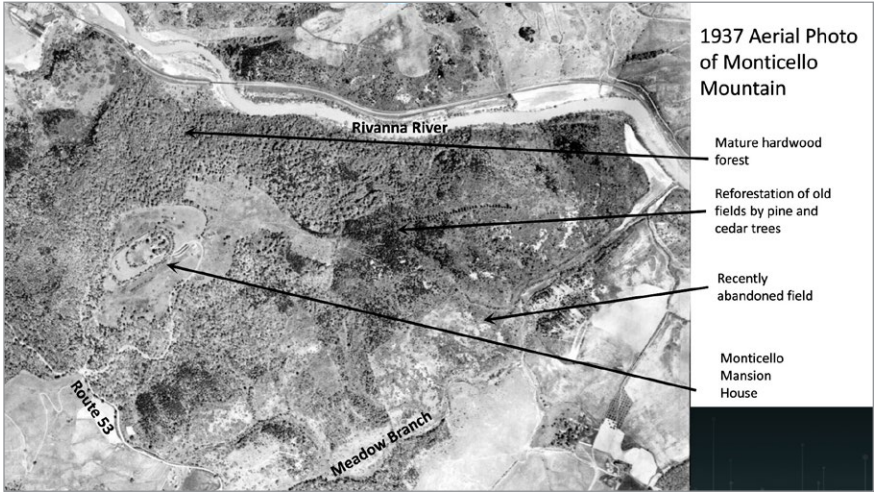
Backdrop

Lidar itself is not new to archaeology, with the first instances of its use in the 1970s when European archaeologists

Did you know there are three Monticellos?

- 1. The mansion house,
- 2. Monticello Mountain (500+ acres), which is one of the plantation quarter farms, and
- 3. The 5000-acre Monticello Plantation.

used it to map castles and surrounding fields. Over the years it has proven particularly useful in regions where dense vegetation hides architectural ruins, for example pyramids, house compounds, and causeways of pre-contact Mayan sites in Mexico and Central America. In the United States, it has been very beneficial at sites like Cahokia near St. Louis, where Native Americans built monumental earthen mounds and plazas. At Monticello,



Aerial photograph of Monticello Mountain, 1937.

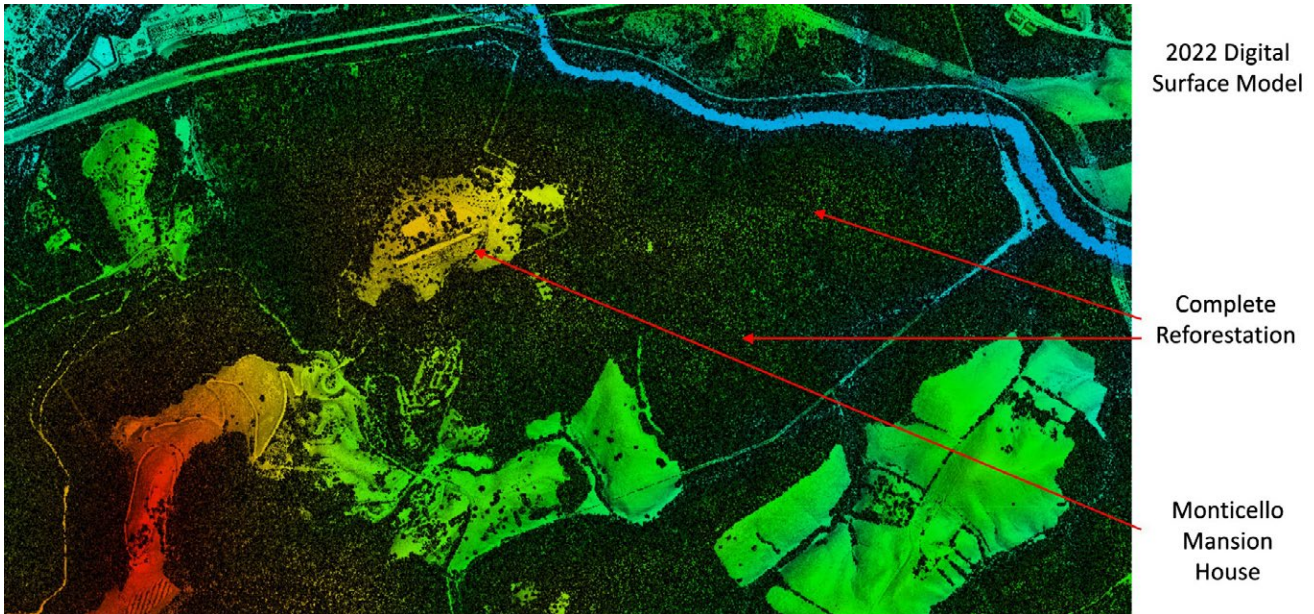
archaeologists are using lidar to advance our understanding of both the massive amount of earth-moving required to construct the ornamental landscape around Jefferson's mansion, as well as subtle and often otherwise invisible features in the plantation landscape.

Modern efforts

At Monticello, modern archaeological research began in 1979 when the Thomas Jefferson Foundation assembled a team to investigate the Monticello mountaintop, including Jefferson's mansion and Mulberry Row, a street

adjacent to the mansion lined with the houses of free and enslaved laborers, as well as the shops and outbuildings in which many of them worked. Beginning in 1997, the Foundation launched the Monticello Plantation Archaeological Survey to explore the rest of the property, where Jefferson's fields and the houses of enslaved agricultural laborers were located. Artifact concentrations indicating where people lived and worked are identified via excavation of shovel test pits dug at 40-foot intervals. Shovel test pits are circular holes 1-foot in diameter that are dug to subsoil, and soil and sediments are screened through 0.25" hardware cloth to reveal artifacts. So far archaeologists have dug 26,000 test pits, covering about a quarter of the Foundation's property, and have discovered 28 archaeological sites.

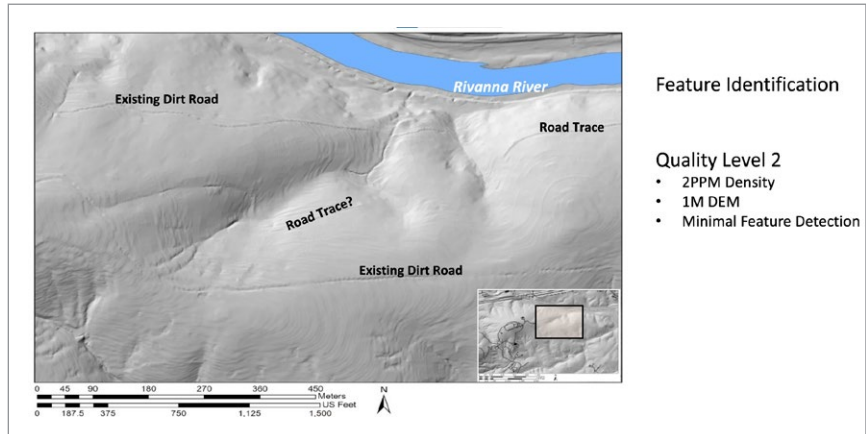
Lidar data is critical because it reveals surrounding landscape features that are not readily seen and identified by



Monticello plantation, the final 2022 DSM revealing the extent of reforestation when compared to earlier data of mixed forested areas and cultivated farmland.

archaeologists working on the ground. The initial data used for this project consisted of 2016 USGS lidar data with 2 points per square meter (ppsm) density and a 1-meter digital elevation model (DEM). While even this low-density data enabled researchers to detect previously indiscernible details in the terrain, it did not provide the level of detail needed for more in-depth analysis. Archaeologists sought to increase the level of detail they could obtain from higher density lidar.

In 2022 the Monticello archaeology team contracted with Surdex Corporation, a geospatial company recognized for its commitment to quality data, for aerial lidar coverage of Jefferson’s original 5000-acre holding to document the ornamental landscape and identify subtle traces of past agricultural



Monticello plantation, 1-meter DEM from 2 ppm lidar revealing roads.

provided some history of previous efforts and discussed the objective of the 2022 project, to identify subtle landscape features that provide a fuller picture of the history of land use on the property.

because, by 2022, a significant portion of the project area had been reforested, obscuring the bare earth for clear lidar returns.

The processed 30 ppsm lidar data produced significantly enhanced digital elevation models with significantly higher clarity than the 2 ppsm USGS lidar that was publicly available. The berm and road trace lines are notably enhanced, and the rows of soil where orchards had been planted (previously undetectable) are readily visible.

The final deliverables for the project were a bare-earth point cloud, a 1-foot DEM, a 1-foot digital surface model (DSM) and a 1-foot intensity image.

“The level of detail that the lidar data provides is astounding—it’s like waking up in the morning and putting on my glasses.”

land use, including berms left by vanished fences and field boundaries, road traces, walls, long parallel ridges that mark orchards, and erosion gullies carved by agricultural runoff. Such features would provide clues for further investigation, including excavation.

Brad Barker, Surdex’s Director of 3D Mapping, flew to Virginia to meet with the Thomas Jefferson Foundation archaeological team, headed by Dr. Fraser D. Neiman, Director of Archaeology, and Derek Wheeler, Research Archaeologist. During the meeting, the archaeological team

Lidar project design and specifications

With the objective laid out clearly, the next step was to design the most efficient acquisition plan that would ensure the desired point density. The project called for the acquisition and processing of 33 square miles of 30 ppsm lidar.

Surdex’s design was to acquire the data with an Optech Galaxy Prime sensor at 1350 feet above ground level. As shown on the flightplan overleaf, there was a total of 25 flight lines at 60% sidelap to ensure complete coverage. Acquisition proved to be challenging

New discoveries

The 2022 lidar data provides important new insights into changing spatial organization and land use at Monticello. Its analytical potential is enhanced by an archive of plats that were surveyed and drawn by Jefferson himself, as he laid out new agricultural fields and roads. Although distorted by survey errors, Jefferson’s maps provide valuable clues to the identity of anomalies seen in the lidar. Later historical maps are also useful. A



Surdex's flight plan to acquire lidar data of the Monticello plantation at a density of 30 ppsm from a flying height of 1350 feet above ground.

1923 survey plat, which shows property lines and ownership from 1833, affords a record of how pieces of Monticello were sold off after Jefferson's death in 1826. Early aerial photos are also important; for example, a 1937 aerial survey by the US Department of Agriculture shows the location of Jefferson's wheat fields that continued in use for a century, soon after they were finally abandoned and reforestation had set in.

The plantation landscape can be divided into two zones: an ornamental precinct that surrounded the mountaintop mansion and the agricultural precinct further down the mountain and across the low hills that surround it.

At the center of the ornamental precinct at the top of Monticello Mountain lay Jefferson's mansion, carefully sited on level ground sculpted by the labor of enslaved workers. Lidar offers superb documentation of the results of their efforts: a perfectly flat surface, parabolic in plan, encompassing an area of two football fields.

Lidar reveals new traces of the "roundabout" road system that documents tell us was constructed in the 1790s. As recorded by Jefferson, enslaved workers cleared four roundabouts circling the mountaintop at successively lower elevations. A series of connector roads linked adjacent roundabouts. The roundabouts

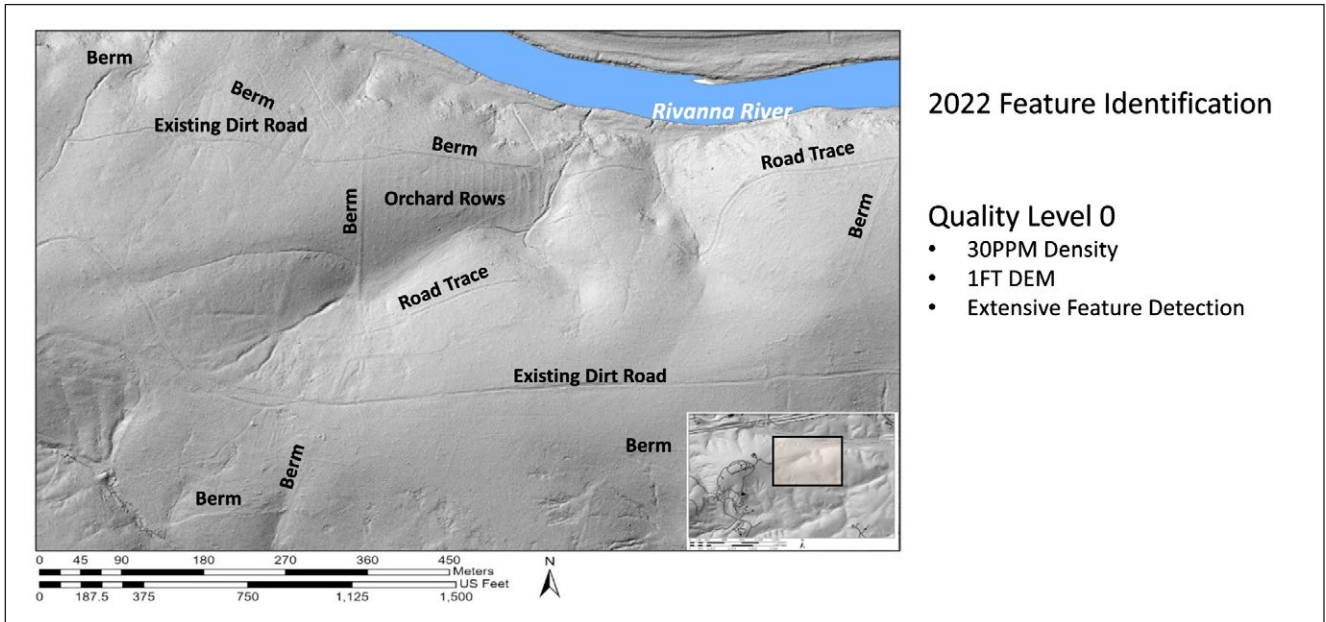
echoed landscape designs Jefferson saw in England on the estates of aristocrats.

Segments of some of the roundabouts and connectors survive and are still in use today.

But many other segments, missed in earlier mapping campaigns, can now be identified in the new lidar data and precisely located on the ground.

Lidar also unveils previously unrecognized segments of what Jefferson called "the north road." This was essentially the "scenic route" that snaked along the contours of the mountain's steep, forested north slope and transported visitors to the mountaintop mansion, out of sight of the plantation's agricultural fields.

Lidar also gives us new insights into two landscape features that fell outside the ornamental precinct but were the source material used to construct the mansion at its center. The first is the brickyard where hundreds of thousands of bricks were made. Lidar uncovers a long, low earthen berm stretching across a flat-bottomed, stream-fed ravine about a half-mile south of the mansion. On the upstream side of the berm the ground level was higher, an indication of impounded sediment behind it. The dam served to collect water required to process the clay for molding. The ground behind the dam was littered with small mounds which field testing revealed as piles of brick wasters (over-fired bricks). Another half-mile to the south, archaeologists identified a stone outcrop and the depression below it where tons of arkose (a coarse sandstone rich in feldspar) were quarried for use in constructing Monticello's cellars and wings.



Monticello Mountain, 2022 bare earth with 1-foot DEM from 30 ppsm lidar revealing significant improvement in resolution over the previous 2 ppsm lidar.

Lidar also provides new evidence of the plantation’s roads on which crops, and the enslaved people who grew them, moved. What Jefferson called the “east road” connected the mansion to the plantation’s fields and the fields to the Rivanna River, which carried crops to Richmond, Virginia, for sale on Atlantic markets. While segments of this road are still in use, there were no traces of it within a half a mile of the mansion. However, archaeologists can see the missing part in the lidar data.

Lidar data divulges yet more physical marks of past land use. For example, long-vanished fence lines left traces in the form of linear berms created by sediment trapped in the vegetation growing under them. The berms are traces of agricultural field and property boundaries. Some of them are visible today on the ground, but others can only be seen in the new lidar coverage. The locations of many berms match

the property boundaries shown on the 1923 survey plat and date back to the division and sale of the plantation after Jefferson’s death a century earlier. However, some of them may mark the edges of Jefferson-era fields.

of these are invisible to an observer standing on top of them.

In the early nineteenth century, at the same time Jefferson was directing his overseers and enslaved field hands to start cultivating wheat as a cash crop, he also

“Archaeologists can decipher how Monticello’s residents altered the environment and had to adapt to these changes. The new lidar data helps identify areas for this kind of scientific investigation.”

The new lidar coverage offers fresh insights into the locations of long-vanished orchards. These appear as parallel ridges averaging roughly 30 feet apart, left by tree rows and well-trodden paths between them. Most

had these same people start additional building projects in an attempt at economic diversification, such as a series of mills along the Rivanna River. These include a grist mill designed to grind wheat into flour for the export trade; a toll

mill that ground wheat and corn which was consumed locally; and a sawmill whose products were used at Monticello and neighboring plantations. The locations of the mills as well as traces of the canals that brought the water to power the mills can be seen in the lidar data.

Laying the groundwork for future research

A major focus of archaeological research at Monticello is the transition from the hoe-based cultivation of tobacco to plow-based cultivation of wheat in the 1790s. Lidar allows archaeologists to identify the effects of the plowing more accurately, including erosional gullies. Not surprisingly, it reveals that gullies are widest and deepest on the southern slopes of the mountain, where the wheat fields were located.

The gullies literally point to another important land-use trace visible in lidar: level areas below them where the eroded sediment was trapped by natural topography or rock walls. Locating trapped sediment opens the door to exciting future research opportunities. In previous work, archaeologists at Monticello discovered that similar erosion deposits are often deeply stratified. The bottom layers pre-date European settlement and are overlain by layers that span initial European settlement and tobacco cultivation, then the transition to wheat, and finally reforestation. By analyzing stratified sediment using a variety of scientific methods (for example, pollen analysis, sediment chemistry, and optically stimulated luminescence dating), archaeologists can decipher how Monticello's residents altered the environment and the ways in

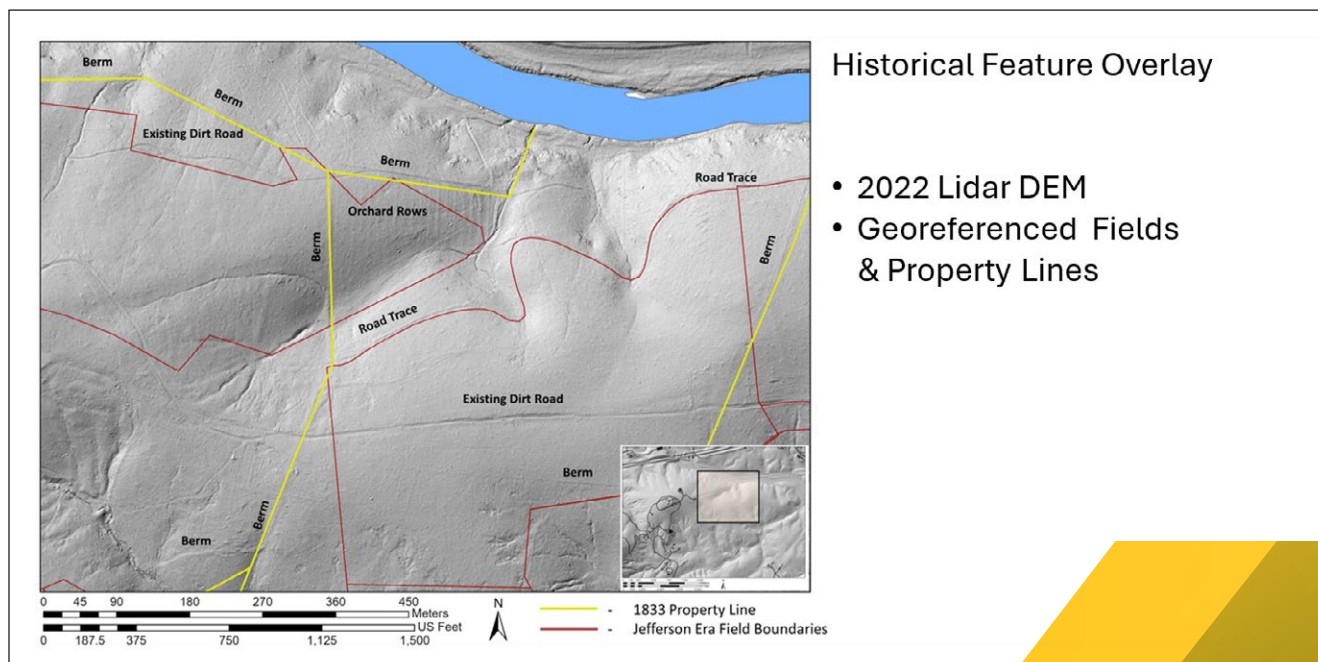
which they had to adapt to these changes. The new lidar data helps archaeologists identify areas for this kind of scientific investigation. **1**



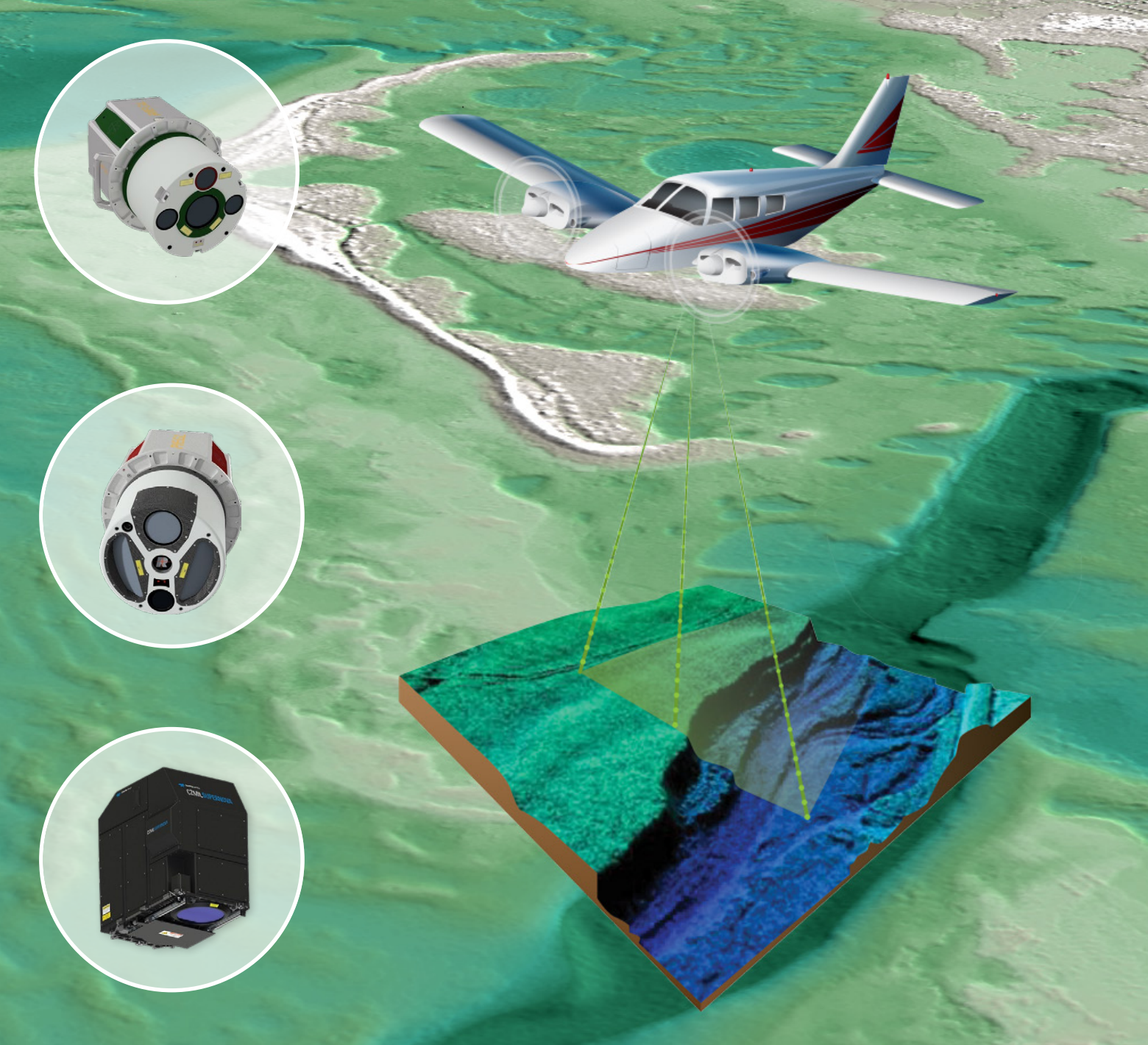
Brad Barker is Director of 3D Mapping at Surdex Corporation, Chesterfield, Missouri, USA. Brad has been with Surdex for 26 years. He has a BASc degree in GIS and cartography from Missouri State University.



Derek Wheeler is a Research Archaeologist at the Thomas Jefferson Foundation, Charlottesville, Virginia, USA. He has been with the Foundation for 29 years. He has a BA in anthropology from the University of California, Berkeley and a MA in anthropology/archaeology from the University of Virginia.



Monticello Mountain: the final 2022 DEM with overlays of the 1833 property lines and early 19th century field boundaries.

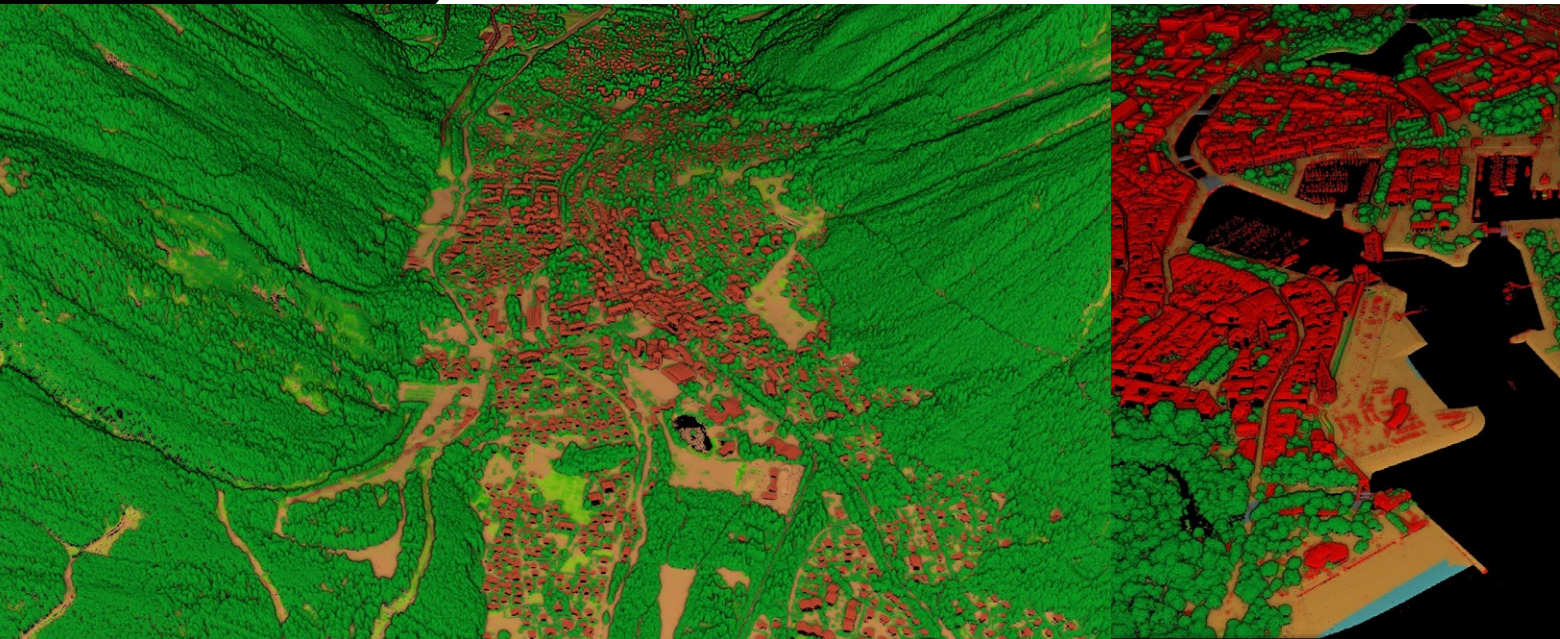


APPLYING THE LATEST TURNKEY SOLUTIONS AND REMOTE SENSING TECHNOLOGY FROM DATA ACQUISITION TO CLIENT DELIVERY

Amar Nayegandhi, CP, CMS, GISP
anayegandhi@dewberry.com
813.421.8642

 **Dewberry**[®]

www.dewberry.com



3D AI in the Lidar HD Production Process

How AI improves the point-cloud classification process at IGN, France's national mapping agency

The Lidar HD program

Designed to meet the needs of various public actions (flood risk prevention, estimation of forest resources, etc.), the Lidar HD program aims to provide a 3D description of the French territory by 2025, using high-density aerial lidar (10 pulses/m²). Operated by the French Mapping Agency (Institut national de

l'information géographique et forestière, IGN) with both internal resources and subcontracted assistance, the project is funded by governmental allocations and regional authorities' support. The data acquired and produced as part of this program is made available as open data (point clouds, DEMs, DSMs, etc.).

The program consists of four phases: data acquisition, processing, hosting and

distribution, and user support. In this article, we focus on the data-processing phase, specifically on point-cloud classification. Point clouds are segmented into ten classes: ground, low, medium, and high vegetation (categorized based on height above ground), buildings, water, bridges, permanent structures (including wind turbines, antennas, high-voltage lines, etc.), artifacts, and unclassified (**Figure 1**).

BY FLORYNE ROCHE

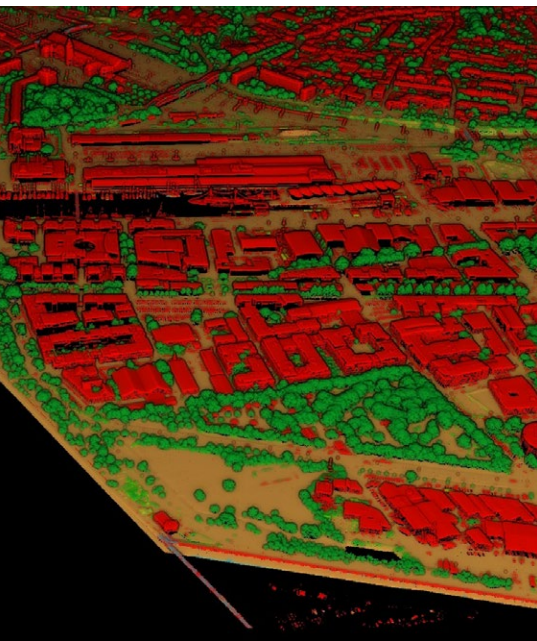


Figure 1: Classified Lidar HD point cloud over the valley of Chamonix (left) and the harbor of La Rochelle (right). The ground is shown in orange, buildings in red, vegetation in shades of green, water in blue.

The area to be processed spans 550,000 km², encompassing mainland France and its overseas territories. This amounts to a massive 3 petabytes of lidar data. The data acquisition and processing are sequenced in blocks of 50 km x 50 km and must be adapted to a range of sensors (Leica Geosystems, Riegl, and Teledyne Geospatial), acquisition seasons (leaf-on or leaf-off), and diverse landscapes (plains, mountains, and overseas territories).

Tools and data for the classification process

Several tools and data sources can be leveraged for point-cloud classification:

- TerraScan¹, a tool from the TerraSolid suite, offers classification routines for classifying the point cloud using explicit instructions.
- Odeon² is a deep-learning library developed at IGN and used

to create CoSIA³, which uses artificial intelligence to produce a large-scale nationwide land cover map⁴, called OCS GE (OCcupation du Sol à Grande Échelle). Based on aerial imagery, it provides a partition of the territory into 17 classes: deciduous and coniferous trees, crops, lawns, bare soil, water surfaces, greenhouses, etc.

- Myria3D⁵ is a deep-learning library designed for multi-class semantic segmentation of large-scale, high-density aerial lidar point clouds. Developed at IGN, it benefited from close collaboration with research teams highly engaged in deep-learning methods for 3D classification. Models trained in Myria3D can predict the probability of each point in a 3D cloud belonging to the classes described above.
- BD Topo[®] is a 3D vector description of the French territory and its infrastructures (buildings, roads, etc.), with metric precision.

1 terrasolid.com/products/terrascan/
2 github.com/IGNF/odeon

The classification process combines these different sources and algorithms, resulting in improved performance compared to relying on a single method.

Two use cases for 3D AI in the process

The classification process is characterized by a sequence of steps (each represented by a TerraScan routine) that must be followed in a defined order (**Figure 2**). In this section, we explore two examples of the use of 3D AI in the process—buildings and ground.

3 cosia.ign.fr/info
4 geoservices.ign.fr/ocsg
5 github.com/IGNF/myria3d

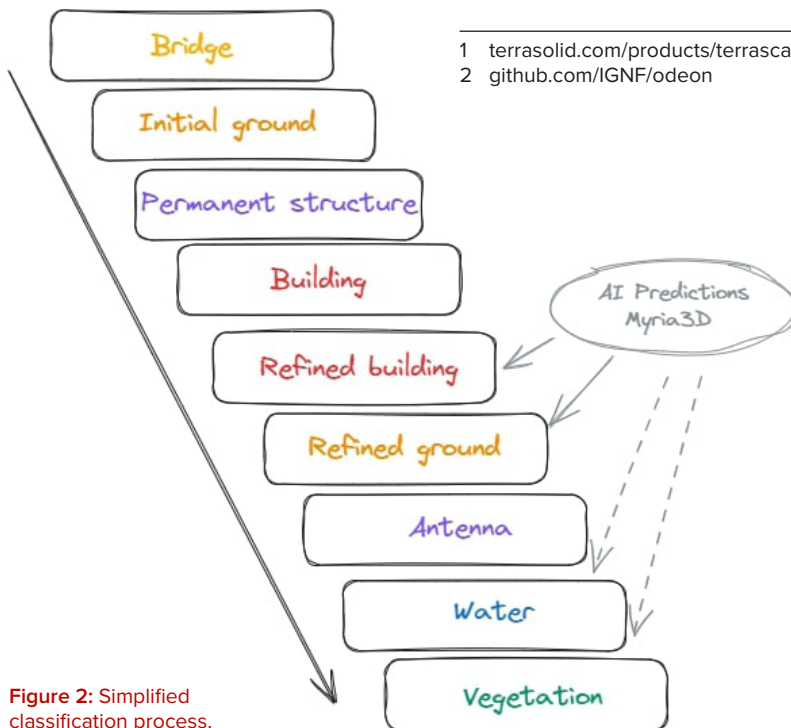


Figure 2: Simplified classification process.

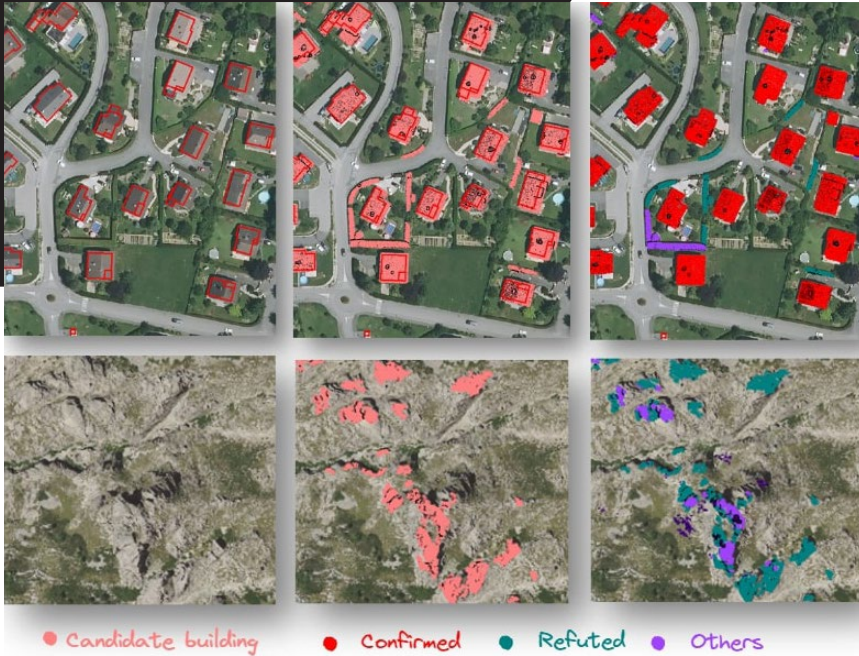


Figure 3: Separation of point groups classified as buildings (pink) into validated (red), refuted (green), or to be verified (purple) buildings.

Building: AI as a validator

The main idea: striking a balance between automated and manual correction

The detection of buildings is clearly crucial. Although explicit routines are used to detect buildings, they often result in over-detection (e.g. trucks, caravans, wood piles adjacent to buildings). Some sort of checking is essential.

If a group of points classified as buildings is located in an area sufficiently covered by buildings in the BD Topo, these points can be excluded from the inspection. Nevertheless, subsequent human verification remains time-consuming, sometimes trivial, and therefore tedious.

To develop a solution, therefore, the production process has been taken into consideration and a module built to be

placed between the automatic detection of buildings and their verification by an operator, with the goal of reducing the number of verifications.

This module is tasked with differentiating between groups of points identified as buildings:

- Those that do not require inspection because the AI, in agreement with BD Topo, is confident that they are buildings
- Those that do not require inspection because the AI, in accordance with BD Topo, is confident that they are *not* buildings
- And those for which the AI cannot make a confident determination.

Only in the case of the third bullet above will the operator be asked to make a verification (**Figure 3**).

Training data: buildings only

In AI, training data is a crucial resource: its availability and quality directly impact model performance. The dataset used to train the first AI model covers various urban and rural landscapes, spanning an area of 150 km², but features a single class: buildings. The points' labels have been verified and curated by operators. As a result, the trained model can predict with considerable accuracy whether or not a point should be classified as a building.

Procedure: optimization under constraint of decision thresholds

The process works on points that are grouped into connected components by proximity (**Figure 4**). For each component, a decision is made to classify it as a building, not a building, or an uncertain case. This decision is based on two sources of truth:

- The point cloud processed by the AI model, giving a building probability *for each point*.
- Building vectors from BD Topo.

The decision is also based on *thresholds*: a point is validated if its probability is *sufficiently* high, and refuted if its probability is *sufficiently* low, and when the proportion of validated (or refuted) points of a component is *sufficiently* high, that component is confirmed (or refuted) according to each of the sources. These decisions are then cross-referenced to apply the final decision to all the points in the connected component (**Figure 5**).

The five decision thresholds used in this process are optimized to maximize automation, i.e. to reduce the number of groups of points to be verified, under the constraint of maintaining fixed

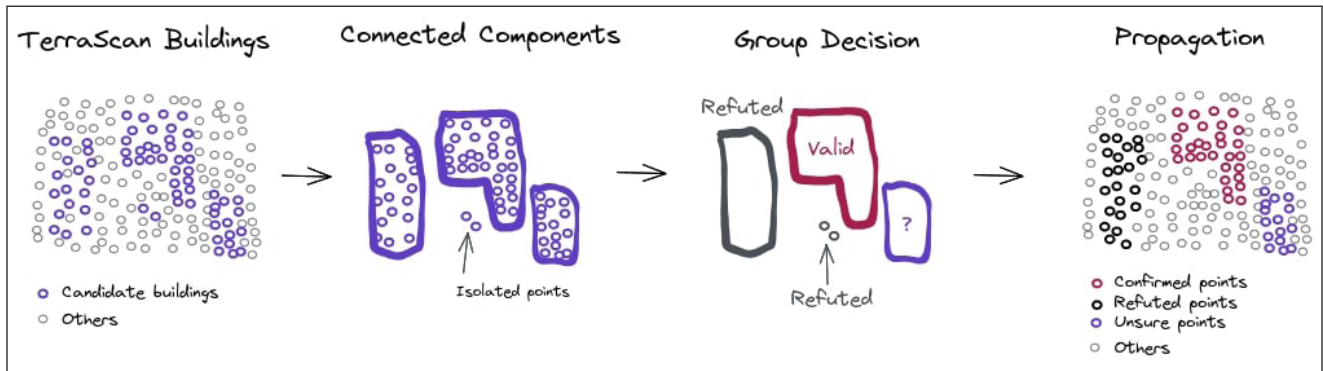


Figure 4: Outline of the building classification assistance module.

quality performance (precision and recall above 98%) (Figure 6).

Results

There is a synergy between the two sources due to the joint optimization of thresholds. AI compensates for the shortcomings of BD Topo, and BD Topo makes up for the erroneous refutations of the AI model.

By January 2022, 85% of point groups could be verified automatically. Since then, continuous improvement of the AI model (multiclass model, variety of training data) has enabled decisions for 96% of point groups to be automated, resulting in a significant reduction in the visual inspection time required to process these uncertainties.

Ground: using AI to fill in the gaps

Classification of points as ground is of major importance too and presents problems of its own. Several of these have been addressed and effective solutions developed.

Ground detection on ridges

Explicit routines for ground detection often struggle to detect ridges. These routines work by densifying low points via triangulation, where ground slopes

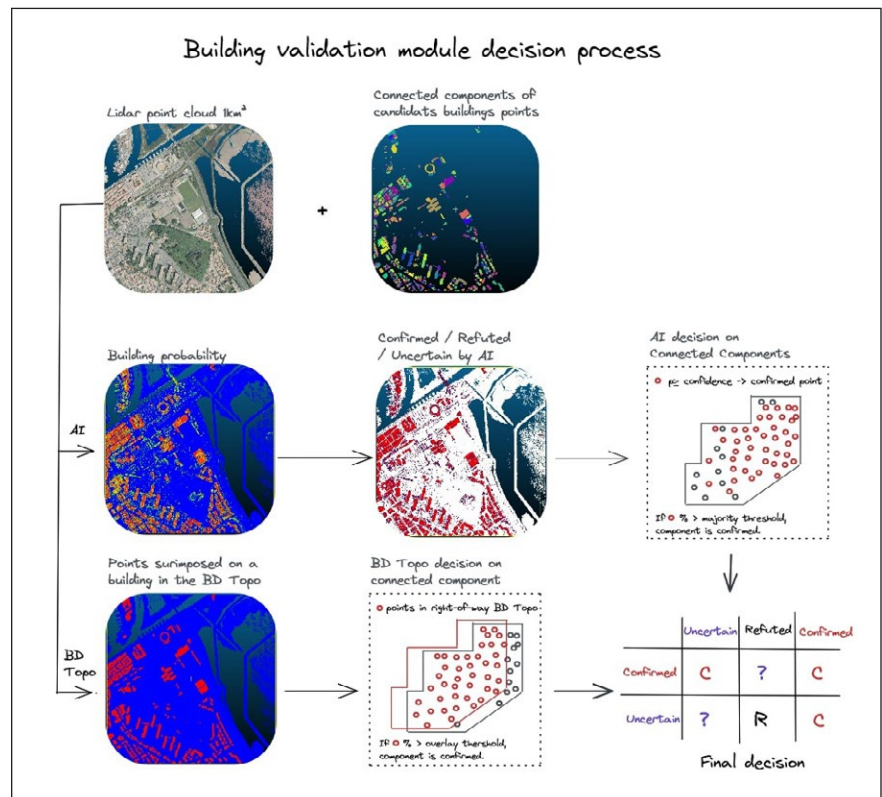


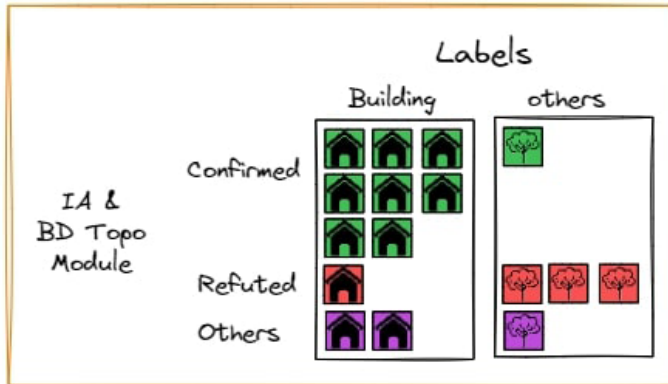
Figure 5: Decision process in the building validation module.

are limited to avoid classifying buildings as ground. However, this approach often fails to detect rocky ridges. As a result, the bare-earth digital terrain model (DEM) can have unsightly triangulations (Figure 7a). The question is whether the 3D AI model can detect ground on these ridges.

Training data: 151 km² multiclass

The model is a multiclass one, trained on a 151 km² dataset spanning three administrative departments. The classification of this area is the result of an automatic process followed by manual corrections. These 151 km² do not include any mountainous areas, but they

Decisions and mistakes



Constraints and requirement to maximize

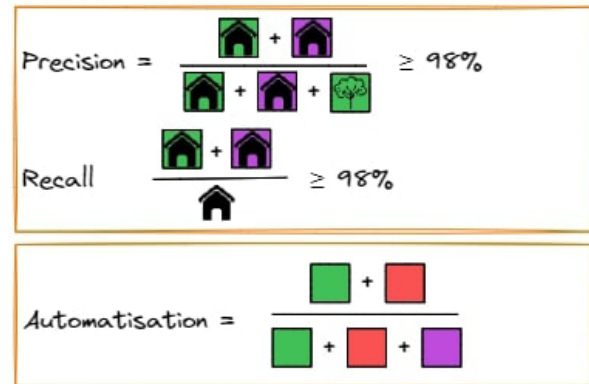


Figure 6: Threshold optimization under constraints.

do include a few square kilometers covering part of the Gorges du Tarn, a canyon several hundred meters deep carved out of limestone by the Tarn River.

Process: bringing out the best in everyone

The results of the AI model are not perfect either: ridges are well detected, but there are artifacts that resemble small rocks (Figure 7b).

Surprisingly, the two approaches are complementary: the AI results are good in areas where the explicit routines perform poorly, and vice versa. Therefore, the decision was made to combine the two sets of results. In cases where the explicit routine yields a low density of ground points, the points classified as ground by the AI model are used instead.

Results: astonishing complementarity

The result (Figure 7c) is surprising: the two sets of data complement each other perfectly, even in the Alps, a mountain range with vertical drops that are much greater than those of the Gorges du Tarn!

Future perspectives: greenhouses, hydrography, vegetation...

Other classes are likely to benefit from the complementarity of the different data sources. Tests are currently being finalized and prepared for deployment to process greenhouses, hydrography, and vegetation using explicit routines based on predictions from Odeon models (2D AI), and Myria3D models (3D AI).

Summary and perspectives

The use of Myria3D, an AI framework designed for 3D processing, has significantly improved results. The use cases described in the previous paragraphs have been in production for over a year.

From the beginning, the decision was made to position Myria3D AI as a supplementary tool to augment other methods (explicit routines) and data sources (BD Topo, OCSGE probability map), leveraging the Institut's expertise in lidar (creation of a cross-disciplinary AI team) and the use of the TerraScan tool to coordinate the various sources.

AI was gradually incorporated into the classification process, according to improvement priorities (buildings, then ground; hydrography, vegetation, and greenhouses to follow), available data, and results (the subject of bridges was not pursued, as the tests conducted did not yield conclusive results).

To contribute to the 3D AI research ecosystem, we have made the Myria3D code open source⁶, and the training dataset for the latest AI model will also be made public soon. Lidar HD data is openly available⁷.

Several perspectives are currently being examined.

- As the Lidar HD program progresses, more and more data becomes available to train our 3D AI models. From an initial situation of scarcity, we now have access to abundant training data. We therefore developed methods to consolidate a highly diverse training dataset via the sampling

⁶ github.com/IGNF/myria3d/

⁷ geoservices.ign.fr/lidarhd#telechargementclassifiees

of 60,000 50 m x 50 m data patches spanning 150 km². The Pacasam tool⁸, developed in-house and open source, contributes to this effort.

- The current architecture of the model is based on research conducted in 2021. Using more recent model architecture, such as Super Point Transformer⁹, may lead us to more energy-efficient AI models with competitive results.
- Experiments have been conducted using Myria3D's architecture to distinguish between different forest species. ■



Floryne Roche graduated with a degree in geomatics engineering from Ecole nationale des Sciences Géographiques, in Marne-La-Vallée, near Paris, and began her

career at the Institut national de l'Information géographique et forestière (IGN), where she developed tools for processing altimetry, particularly from lidar data. For seven years, she served as the technical link between the users of IGN products and services and the Institut, gaining a deep understanding of the business needs of her contacts. Currently, as Product Owner of the AI team within the Lidar HD program, she ensures that AI is effectively integrated into the production process, while also working to promote a clear understanding of its contributions.

⁸ github.com/IGNF/pacasam

⁹ github.com/aamsoftware/official_superpoint_transformer

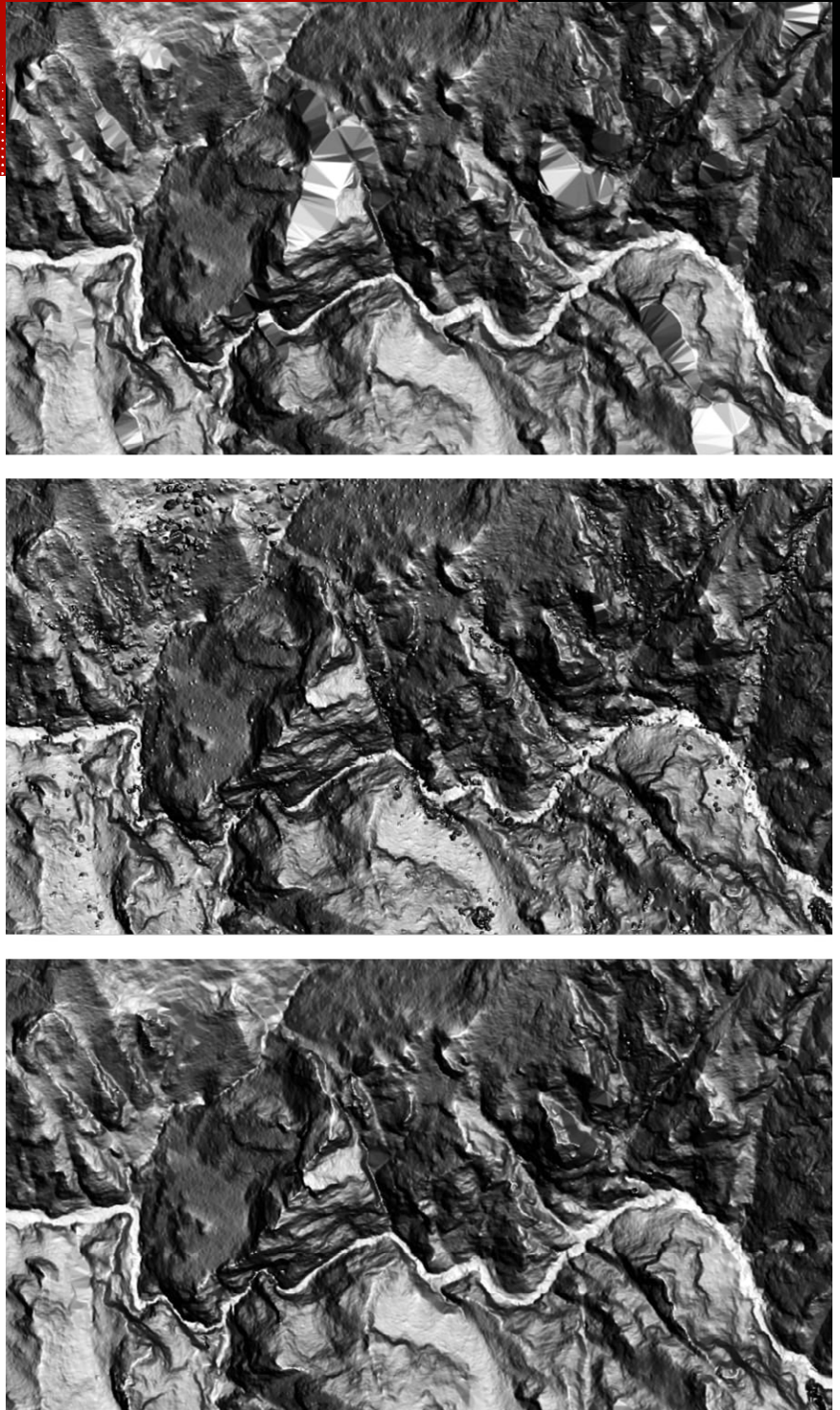


Figure 7: DEM from points classified as ground by (a) explicit routines, (b) Myria3D AI, (c) combining the two sets of results.



Advanced technology is used to map one of nature's most complex creations—the tropical rainforest.

Digital Twins Open Up New Possibilities For Rainforest Conservation

R-evolution uses Hexagon airborne and terrestrial lidar sensors as fundamental data sources

Imagine a digital twin. Perhaps you are imagining the digital representation of a chip inside a phone or of a manufacturing shop floor, perhaps you are picturing a Formula One race-car engine or even an entire digitized city. Now imagine using this capability for a rainforest in Costa Rica where jaguars and tapirs roam and exotic birds perch in ancient and medicinal trees.

Advanced technologies are now being applied to map one of nature's most complex creations—the tropical rainforest. Hexagon's green-tech subsidiary, R-evolution, recently launched Green Cubes, an initiative which combines technology, science, and environmental

stewardship to revolutionize rainforest conservation. The biodiverse ecosystem of the La Gamba biological corridor (COBIGA), Costa Rica, is being captured with high-precision airborne and terrestrial lidar scanners from Hexagon, to measure and virtually visualize it for continuous monitoring and trustworthy conservation.

Lidar technologies provide a unique opportunity to identify the complexity of the rainforest canopy. The digital twin combines airborne and terrestrial lidar data to unveil the forest in intricate detail and unlock new opportunities to manage the world's natural wonders sustainably.

In an initial partnership with La Gamba Tropenstation, an Austrian research

BY ANDREW **KERR**



The Leica CountryMapper combines a large-format photogrammetric camera with a high-performance lidar unit into a single system to collect imagery and lidar over very large areas simultaneously.

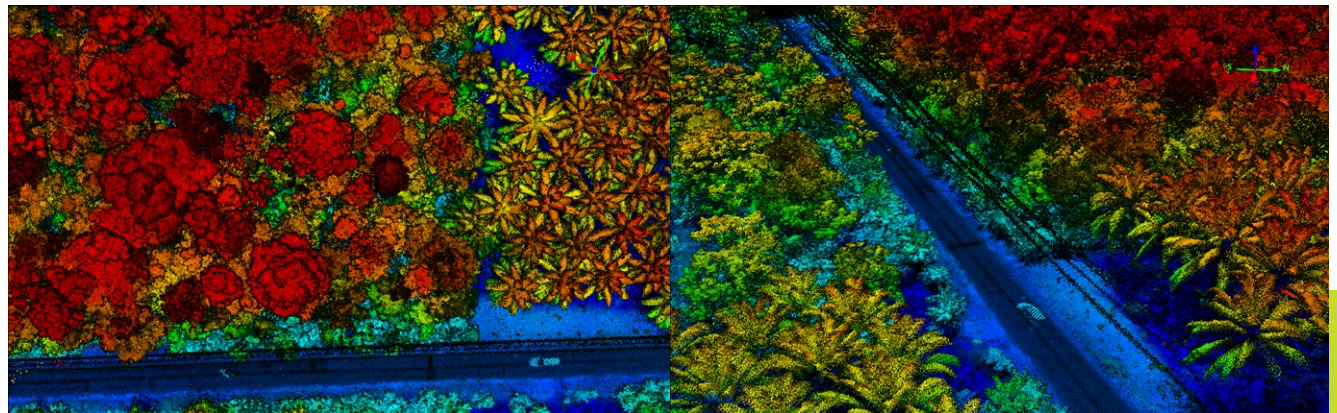
station associated with the University of Vienna, R-evolution is mapping 500 hectares to generate the first 125 million Green Cubes—a sponsorable asset that corporate sponsors can purchase to differentiate themselves through proactive contributions to biodiversity conservation and to meet ESG¹ requirements.

Building the digital twin from the air

Through the combination of airborne and terrestrial lidar with ground sensors, imagery and GIS data, the rainforest's



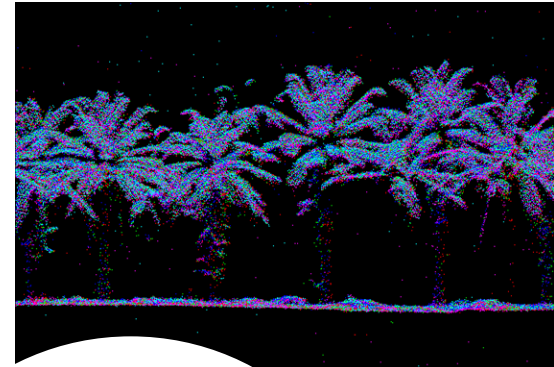
This view gives an impression of the biodiverse ecosystem and dense vegetation in the verdant La Gamba biological corridor (COBIGA), Costa Rica.



These vertical and oblique views of the point cloud from the airborne lidar data, colored by height, give an idea of the detail that the Leica CountryMapper provides.



Andrew Kerr, forest lead at R-evolution, uses the Leica BLK2GO handheld terrestrial lidar sensor to capture data that will be combined with the airborne data to generate a remarkably detailed and precise representation of the rainforest.



Point cloud generated from the Leica BLK2GO data. All the other images to the right show airborne data.

development can be monitored over time with unprecedented precision.

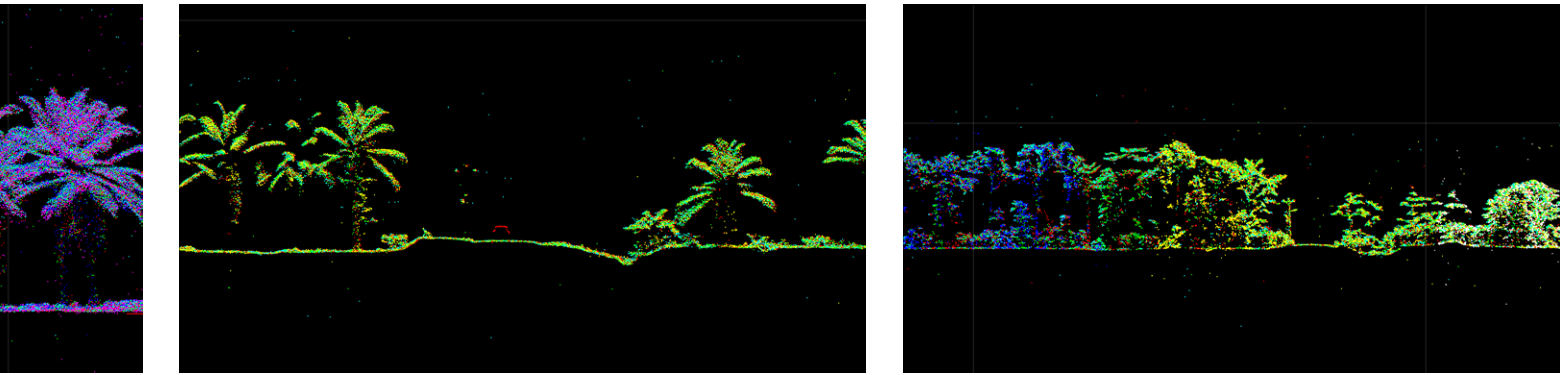
The core of this approach relies on state-of-the-art hybrid airborne sensors from Hexagon. Green Cubes utilizes the Leica CountryMapper hybrid airborne system, which combines lidar and large-format imagery in a single sensor.

The data collected with the hybrid sensor allows the creation of a 3D digital landscape of the rainforest to quantify its volume and to monitor changes in vegetation growth over time. This establishes a baseline for understanding the forest structure. The Leica CountryMapper image data in multiple

spectral bands is registered with the lidar data. As a result, a detailed picture of the rainforest canopy emerges and an index of the different species can be constructed.

Beneath the canopy

The handheld terrestrial lidar scanner, Leica BLK2GO, is applied beneath the canopy to provide high-resolution data for ground-truthing that improves the quality of the forest structure measurement and sets new standards for measuring and analyzing tree biomass volume and diameter measurements while reinforcing the data captured from the air. In addition, data captured by the Leica BLK2GO unlocks a virtual experience for corporate sponsors, bringing nature closer to business.



The combination of data captured with airborne and mobile mobile mapping technologies helps scientists to better understand and monitor the rainforest.

From tape measures to digital twins

The COBIGA corridor work began more than thirty years ago to link the lowland rainforests of Golfo Dulce with the mountain rainforests of Fila Cal in Costa Rica to prevent forest fragmentation and genetic isolation. From 1993 onwards, the team, led by biodiversity researcher Dr. Anton Weissenhofer, always implemented some form of monitoring. Research teams would periodically measure the trees, recording the diameters using tape measures and notebooks.

The team upgraded its equipment as technology progressed. With a small sensor, it could measure the forest in a three-dimensional picture. That provided a good solution, but the data was so massive and unstructured that they were unable to leverage it well.

Now, with Green Cubes and a complete digital twin, visualized using HxDR², it is possible to capture digitally not only the cubic volume of the forest, but also the structure, height, and diameter of the trees in order to calculate the biomass of the rainforest.

Through Green Cubes, researchers can explore the data in vivid detail. They can create virtual tours, take measurements, and add annotations.

The scientists can engage with the captured reality in a much more meaningful way by navigating through point clouds, meshes, models, and other data. Visualizing the data in this streamlined, user-friendly way allows scientists to accelerate scientific progress through enhanced insights and collaboration.

Enabling the change we want to see

Every day, countries, companies and citizens have the opportunity to make positive change. As climate change escalates into an existential threat, we can adopt habits such as reducing waste and water, cutting carbon emissions, and eliminating single-use plastics. Beyond the changes we make, however, we also have a responsibility to enable the change we want to see in the world.

With advanced solutions like digital twins, we can quantify and visualize natural environments in entirely new ways to enhance conservation efforts.

By leveraging lidar to replicate delicate rainforests virtually, this initiative opens new possibilities for sustainability. It embodies how cutting-edge technologies can empower humanity to enact the systemic change required to protect our planet. All our choices matter greatly, but we must also harness technology's transformative power to build a sustainable future. ■



Andrew Kerr is forest lead at R-evolution, Hexagon's division responsible for nature-based solutions, and is heading up the Green Cubes program. He has a background in GIS and digital management together with on-the-ground field experience. His projects have taken him from satellite tracking of wild dogs in Southern Africa to reforestation in Borneo, radio tracking of golden bamboo lemurs in Madagascar and scanning tropical rainforests in Costa Rica.

2 <https://hxdr.com/>

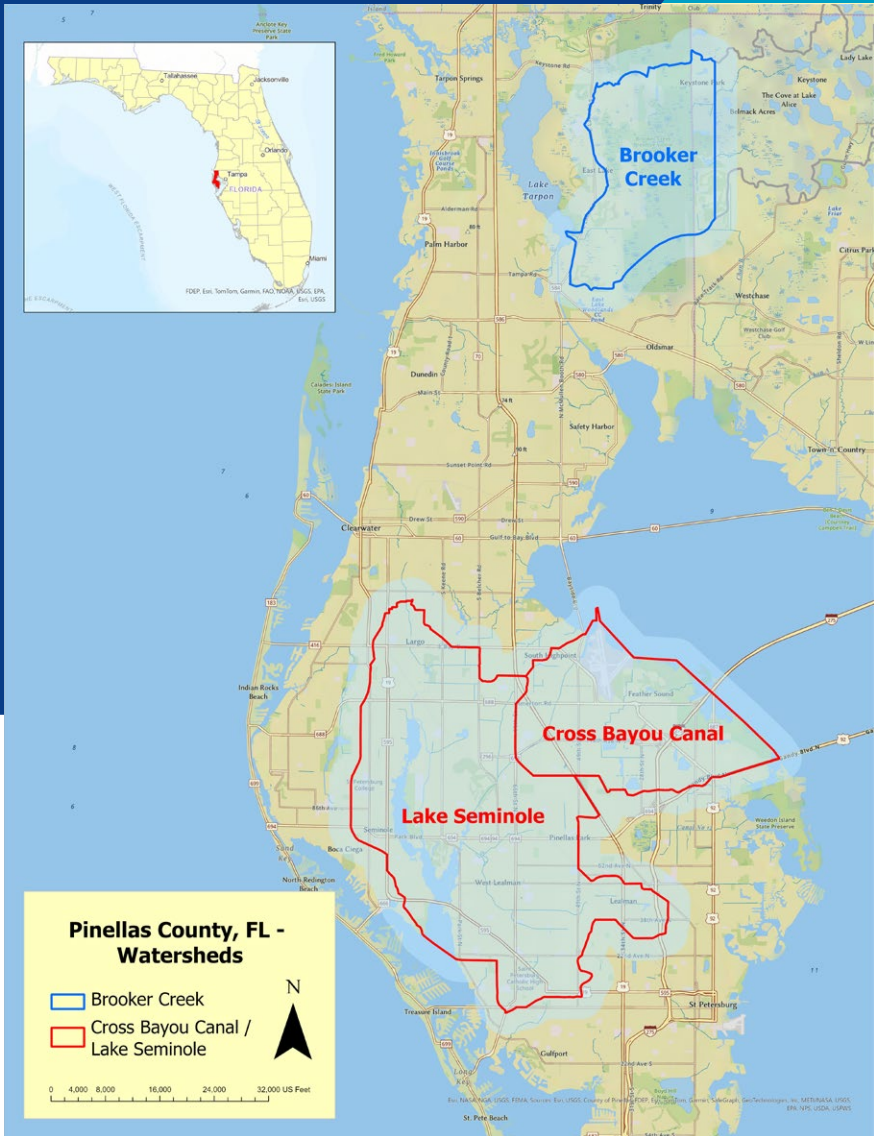


Figure 1: Pinellas County, Florida, showing the northern, mostly undeveloped Brooker Creek watershed and the southern, highly urbanized Cross Bayou Canal/Lake Seminole watershed.

A comparison of different lidar acquisitions in Pinellas County, Florida

Surface-water modeling from lidar-derived DEMs

Over the past 20 years, lidar-derived digital elevation models (DEMs) have become the staple of surface-water hydrography and hydraulic (H&H) modeling. During this same period, lidar has evolved significantly in terms of both absolute three-dimensional (horizontal and vertical) spatial accuracy (<10 cm), and increasing pulse density (>24 pulses per meter square (ppsm)). Most recently, in the commercial lidar market, two distinct lidar technologies have emerged, linear-mode (LM) and Geiger-mode (GM), each with distinct advantages and disadvantages (Lin et al., 2022).

In parallel with the evolution of lidar specifications and technologies, surface-water feature extraction from digital elevation models has also developed. Since the early 2000s the standard methodology for feature extraction involves computing a flow-direction raster and a flow-accumulation raster (Tarboton et al., 1991). While the basic framework has not changed, the methodology for computing these rasters has evolved, from the “D8” method to a multi-directional flow method, to a “D-infinity” method and most recently to a continuous flow A^t methodology (Ehlschlaeger, 1989). The continuous flow model is currently favored by USGS for the 3D

Lidar DEMs for Continuous Flow Surface Hydrography Feature Extraction

BY ALKARLIN

Hydrography Program for the Nation (3DHP FTN)¹ for updating the National Hydrography Dataset (NHD) and the Watershed Boundary Dataset (WBD) using USGS 3D Elevation Program (3DEP) products. The current USGS standard for updating the NHD/WBD to 3DHP is to reevaluate on a watershed (Hydrological Unit Code 8) by watershed basis.

Collecting lidar data over entire watersheds can be a costly proposition, so it is difficult to find watersheds that (1) have been maintained over a sufficient time period with little anthropogenic change, and (2) have been surveyed multiple times with differing lidar specifications and technologies. Fortunately, Pinellas County, Florida provides such an opportunity.

The Southwest Florida Water Management District (SWFWMD) houses the Watershed Management Program with responsibilities including stormwater and flood management in the county. Watersheds are reviewed on a rotating five-year maximum interval basis. In the winter of 2007, SWFWMD partnered with the Florida Division of Emergency Management (FDEM) to collect lidar data for the entire county using a Leica ALS40 LM lidar sensor. Then, in 2013, the 2007 lidar data was upgraded to the USGS QL2 standard with some reprocessing and increased breaklining. The county was re-mapped in 2016, with Harris GM technology, and again in 2019, with newer, dual-channel, RIEGL VQ-1560 II LM technology to meet the USGS QL1 and SWFWMD specifications.

As Pinellas County is the most densely populated county in Florida

with 3425 people per square mile², the urbanized areas have remained as highly urbanized areas over the 12-year period and the non-developed areas, designated as nature preserves, have remained as natural areas. For this comparative study, two representative watersheds in Pinellas County were chosen. Cross Bayou Canal/Lake Seminole is typical of urbanized watersheds with a mixture of industrialization and dense population. The terrain includes extensive ditching/berms and infrastructure for stormwater management. Brooker Creek watershed, which stretches across Pinellas and Hillsborough counties (see **Figure 1**), however, represents “preserved”, more natural portions of the county. The study was restricted to the Pinellas County portion of Brooker Creek, since it has been repeatedly surveyed.

The watersheds

SWFWMD has developed a set of planning units that are used for watershed management and are loosely based on USGS WBD Code 12 HUCs. The SWFWMD planning units, however, also serve as governmental/regulatory units.

For this comparison, two SWFWMD watersheds were chosen to represent the terrain extremes found in the county. The Brooker Creek watershed (**Figure 1**) encompasses a total of 39.44 square miles (25,645 acres), of which only 17.96 square miles (11,681 acres) are in Pinellas County. This area consists of mostly unaltered terrain with the Brooker Creek Preserve accounting for over 8700 acres surrounded by low-density housing.

The second watershed, in southern Pinellas County, Cross Bayou Canal/

Lake Seminole (**Figure 1**), encompasses 71.75 square miles (45,918 acres) in the most densely populated southern portion of the county. In contrast to Brooker Creek, this watershed is highly urbanized, with extensive ditches, culverts, pipes and other infrastructure systems to protect the dense population from stormwater and flooding.

Digital elevation models

Three lidar-derived DEMs were used for this study. For each, the lidar point cloud and polygonal breaklines (waterbodies over 0.25 acres and double-line drains over 8’ wide) were used to construct a hydro-flattened DEM; single-line drains (SLDs) and/or connectors were not used to hydro-enforce the DEM. DEMs were constructed with 2.5’ x 2.5’ cells and tiled according to the Florida Department of Revenue 5000’ x 5000’ tiling scheme.

1. USGS/QL2 (2007/2013): constructed from lidar data originally collected in 2007 and reprocessed in 2013. The data was collected at 2 ppsm in 2007 to the USGS QL2 specification, with breaklines approximately to the *Lidar Base Specification Version 1.0*³. The data was then reprocessed by SWFWMD in 2013 with upgraded polygonal breaklines, as described above.
2. GM (2016): constructed from GM data collected in 2016 by Pinellas County at a pulse density of 20 ppsm with breaklines to meet the SWFWMD polygonal breakline specifications, as described above.
3. USGS/QL1 (2018). As part of the USGS/FDEM Florida Peninsular Lidar Survey, Pinellas County was remapped in 2018. The data was

1 3dhp-for-the-nation-nsgic.hub.arcgis.com/

2 pinellas.gov/about-pinellas-facts/

3 pubs.usgs.gov/tm/11b4/Version1.0/TM11-B4.pdf

collected to meet the USGS QL1 specifications (8 ppsm) with USGS *Lidar Base Specification v. 2.0*⁴ breaklines. SWFWMD upgraded the breaklines to the SWFWMD specifications for polygonal breaklines, as described above, in 2019-20.

Ground-Truth control data

Since 2003, SWFWMD has been using lidar data in support of the Watershed Management Program. In 2007, it started codifying the lidar specifications to support watershed H&H modeling. The *SWFWMD Lidar Surveying and Mapping Specification Template 5.2* (9 August 2022: available upon public records request to SWFWMD) includes breakline specifications that are significantly more rigorous than those found in the USGS *Lidar Base Specification*: (1) all channelized hydrographic features less than 8' wide are captured as 3D single-line, monotonic drains; (2) all channelized hydrographic features greater than 8' wide are captured as 3D double-line and polygonal monotonic drains; (3) all waterbodies greater than 0.5 acres are captured as single-elevation 3D features; and (4) all islands over 0.5 acres in waterbodies are captured as 3D single-elevation features. The SWFWMD specifications also include “connectors”—2D features used to maintain surface water connectivity through breach areas. Connectors could include pipes, culverts, and other non-visible breaches. Where breaches occur along double-line drains, two connector lines are used to represent the breach. Where breaches occur along SLDs, one connector line is used to represent the breach.

⁴ [usgs.gov/media/files/lidar-base-specification-v-20](https://www.usgs.gov/media/files/lidar-base-specification-v-20)

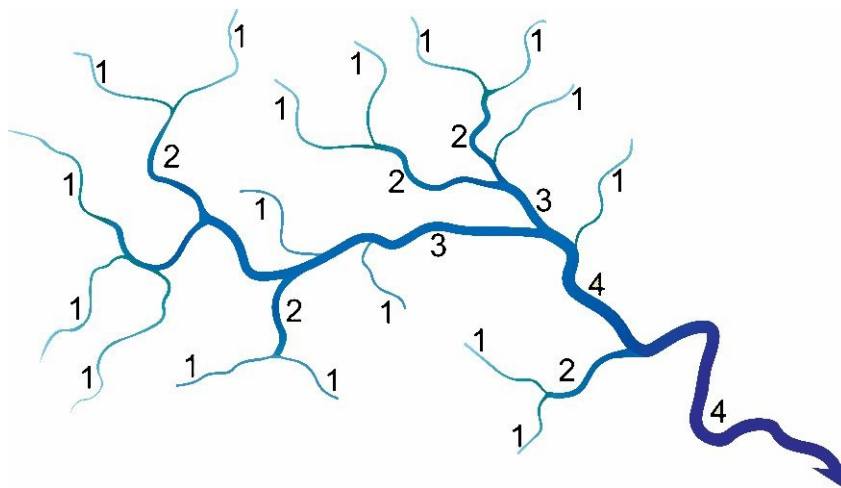


Figure 2: Strahler (1952) stream ordering hierarchy where the smaller streams (order 1) flow into consecutively larger (order 2) streams, and so on.

DEM preprocessing

As the continuous flow A^t algorithm (Ehlschlaeger, 1989) is a cost-based one, standard practice does not include prefilling the DEM to remove sinks and other artifacts in the surface. Similarly, no smoothing was performed on the hydro-flattened DEMs. Nonetheless, two Esri Arc Hydro tools for DEM manipulation were used to preprocess each DEM:

1. To ensure that artificial path connections through waterbodies maintain a valence no greater than three, the double-line drains (polygons) were merged with the waterbody polygons and the Burn Flat Polygons into DEM tool in Arc Hydro was used to re-enforce these areas into the DEM.
2. Where the connectors, i.e. breaches or culverts, were represented as paired linear features, one of the pairs was removed, the remaining member repositioned to the center of the breach/culvert, and the single-line connectors were enforced into the DEM using the Burn Lines into DEM tool.

Analytical processing

With the possible exception of USGS/NHD artificial paths (through waterbodies), the SWFWMD SLDs represent the channelized hydrological features under 8' wide and should agree closely with the channelized features identified for the 3DHP update for the NHD. For this comparison, Esri ArcGIS Pro was used to buffer the SLDs by 5' and the resulting polygons were used to select the results of the flowlines modeled from each of the three DEMs. The linear distance of SWFWMD SLDs, the ground-truth, and the elevation-derived hydrography (EDH), i.e. the modeled channel, were then used to determine the degree of agreement between SWFWMD ground-truth and the modeled EDH results.

Two levels of analysis were performed to help evaluate the differences between the lidar-derived DEMs. Firstly, the lengths of each Strahler stream order were computed and compared to each other, exclusive of the SWFWMD ground-truth. The goal was to

determine the extent of agreement among the lidar-derived DEMs for Strahler orders 1–4. The second analysis entailed using ArcGIS Pro to “select” the stream network as derived from each DEM for comparison to the SWFWMD ground-truth network.

3DHP modeling approach

An ArcGIS Pro workflow focusing on the continuous flow A^t algorithm was developed. The Derive Continuous Flow (Spatial Analyst) tool was used to construct the flow-direction and flow-accumulation rasters from each of the three DEMs. The stream raster network was derived from these rasters using a flow accumulation of 6 acres (261,360 square feet) and specifying Strahler stream ordering (see **Figure 2**; Strahler, 1952) using the Derive Stream as Raster tool. The stream raster network was vectorized using the Stream to Feature tool and the flow-direction raster that was previously generated (**Figure 3**).

Results and discussion

The analysis of the resulting flowline networks focused on two aspects: (1) the numbers and lengths of Strahler order 1–3 reaches (see **Figure 2**), as these represent the SLDs and channels that would be represented in the EDH updates, and (2) the agreement between the modeled flowline networks and the SWFWMD ground-truth.

Flowline network composition (number and length)

As expected, the flowline network composition was similar for each DEM-type for both watersheds. In the non-disturbed Brooker Creek watershed, there was a slight tendency for more flowlines to be observed in Strahler orders 1–3

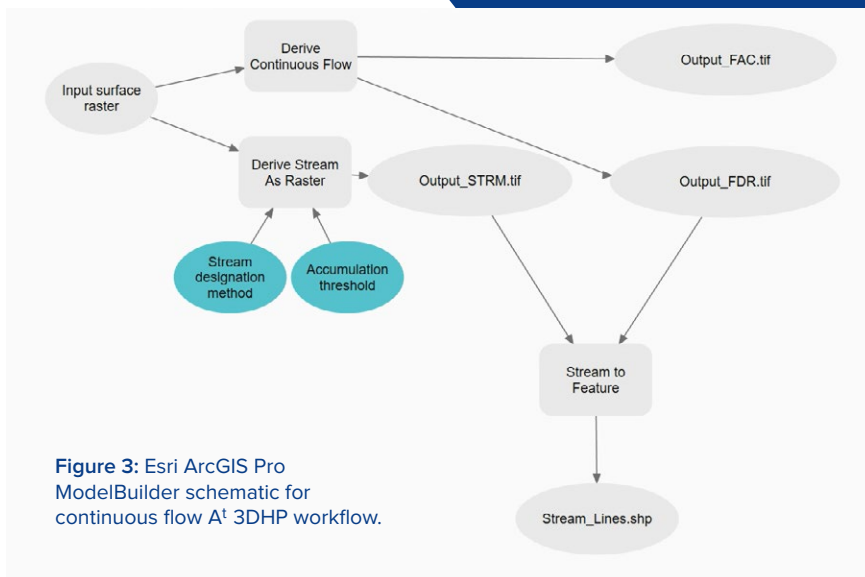


Figure 3: Esri ArcGIS Pro ModelBuilder schematic for continuous flow A^t 3DHP workflow.

BROOKER CREEK			
DEM type	USGS/QL2 (LM)	GM	USGS/QL1 (LM)
Strahler order 1: <50 m (164')			
Number of reaches	90	82	66
Linear miles	1.2	1.2	1.1
Average length (feet)	71.4	78.2	82.4
Length range (feet)	1.2 – 160.6	0.8 – 159.9	1.2 – 162.8
Strahler order 1: all lengths			
Number of reaches	544	570	559
Linear miles	103.9	116.1	113.6
Strahler order 2			
Number of reaches	268	301	277
Linear miles	55.6	60.8	69.5
Strahler order 3			
Number of reaches	152	156	151
Linear miles	35.6	36.1	36.5
Totals (orders 1–3)			
Number of reaches	964	1027	987
Linear miles	195.1	213.0	219.6

Table 1: Numbers of flowlines and length statistics for Strahler stream orders 1-3 derived from three different DEMs for the Brooker Creek watershed.

from the GM-derived DEM relative to either of the LM-derived DEMs (Table 1). However, the total number of linear miles of reaches modeled is slightly larger from the QL1 LM-derived DEM, 219.6 miles, than from the QL2 LM- or GM-derived DEMs, 195.1 and 213.0 miles respectively.

Curiously, although the network composition metrics for the small, Strahler order 1 reaches, i.e., those that are below the USGS/EDH length threshold (50 m; 164'), totaled approximately the same length among the DEMs (~1.1 miles), the QL1-derived DEM resulted in 26% fewer flowlines than the QL2-derived flowlines and almost 20% fewer lines

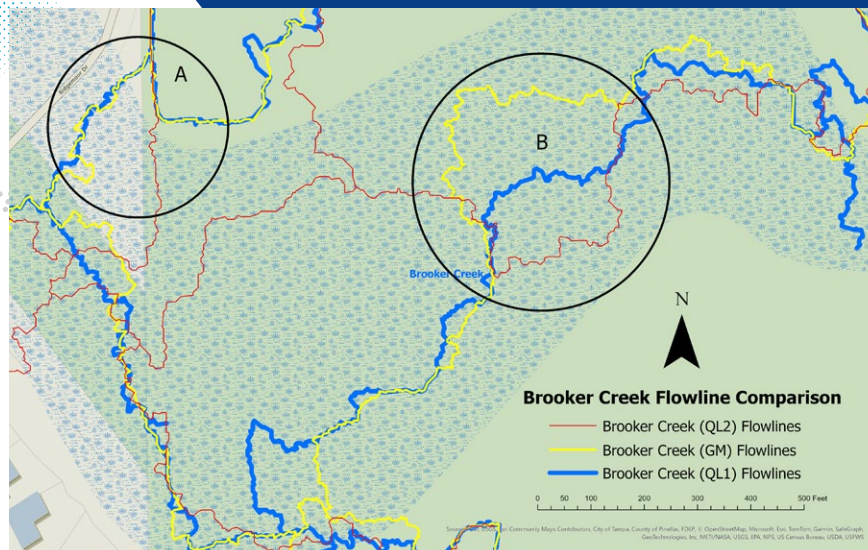


Figure 4: Comparison of flowlines in wetlands at Brooker Creek Preserve, derived from continuous flow modeling: (A) area of close similarity between the QL1- and GM-derived flowlines; (B) area of divergence between the three DEM-types.

than the GM-derived flowlines. Nevertheless, although the average length of the flowlines modeled from QL1-derived DEMs was larger than either the QL2- or GM-derived DEMs,

the difference between any was not significant ($F_{2,235} = 0.96, p = 0.38$).

In Cross Bayou Canal/Lake Seminole too, the three lidar-derived DEMs produced similar network metrics for Strahler orders 1-3, with the USGS/QL1 DEM resulting in the longest flowline network: 718.1 miles compared to 702.6 miles and 706.9 miles for the QL2 and GM-derived flowline networks respectively (Table 2). Again, the slight differences in combined flowline length cannot be attributed to the difference of the lidar-derived DEMs.

In this urbanized watershed, however, the between-DEM variance for stream length in the small Strahler order 1 flowlines less than 50 m is significantly different ($F_{2,1022} = 5.15, p = 0.005$), indicating that the length of the small upper reaches is dependent on the original DEM used for the modeling, the LM-derived DEMs yielding longer upper-level reaches than the GM-derived DEM.

Flowline network geometry

While the flowline network composition metrics do not show significant differences that could be attributed to the underlying DEMs, their spatial geometries, especially in wetlands, are considerably different. As an example, in

CROSS BAYOU CANAL/LAKE SEMINOLE			
DEM-type	USGS/QL2 (LM)	GM	USGS/QL1 (LM)
Strahler order 1: <50 m (164')			
Number of reaches	307	349	369
Linear miles	5.1	4.9	5.6
Average length (feet)	86.8	75.4	79.7
Length range (feet)	7.5 – 163.6	5.3 – 163.9	3.7 – 163.7
Strahler order 1: all lengths			
Number of reaches	2305	2313	2348
Linear miles	398.8	393.6	400.0
Strahler order 2			
Number of reaches	1152	1140	1198
Linear miles	205.5	206.6	216.7
Strahler order 3			
Number of reaches	576	575	543
Linear miles	98.3	106.7	101.4
Totals			
Number of reaches	4033	4028	4089
Linear miles	702.6	706.9	718.1

Table 2: Numbers of flowlines and length statistics for Strahler stream orders 1-3 derived from three different DEMs for the Cross Bayou Canal/Lake Seminole watershed.

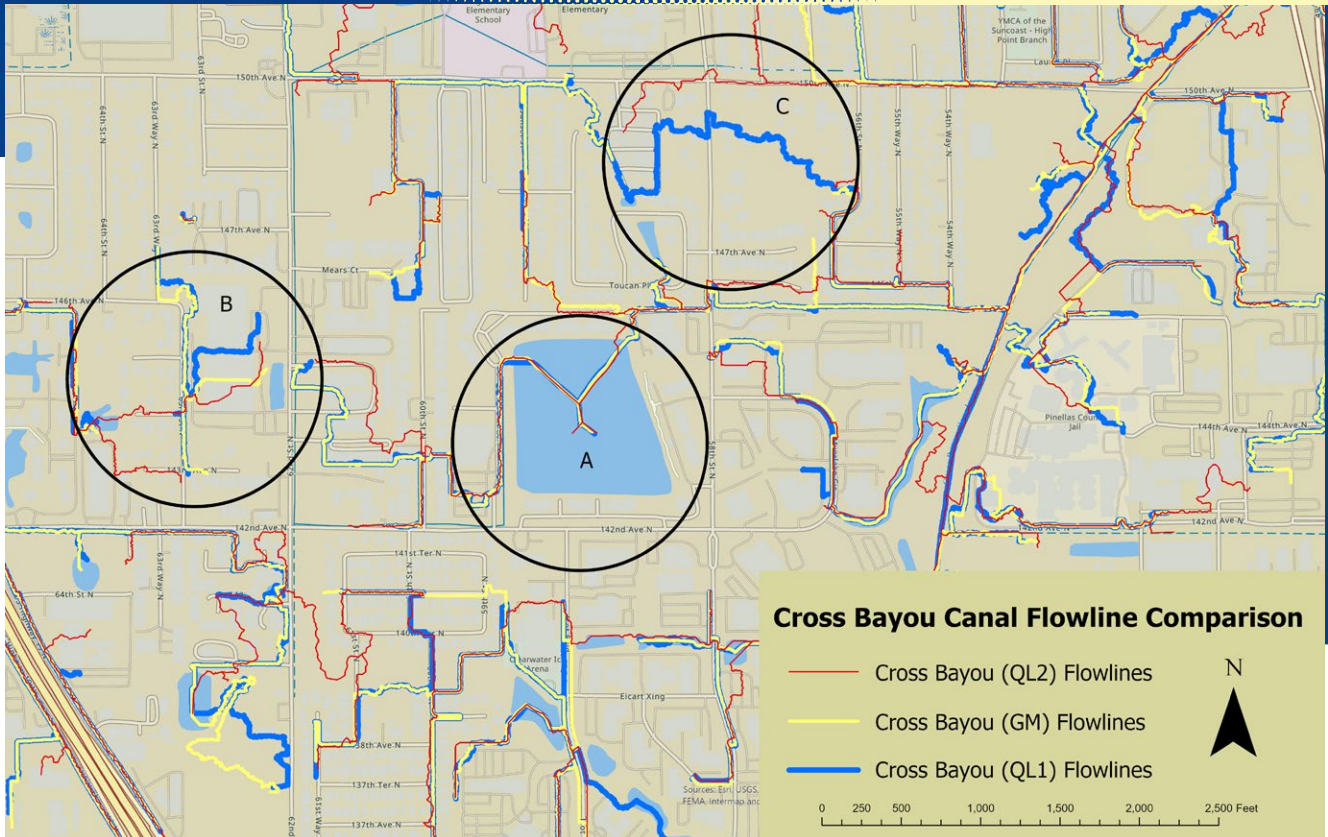


Figure 5: Comparison of flowlines at Cross Bayou Canal/Lake Seminole, derived from continuous flow modeling: (A) - area of close similarity between the QL1- and GM-derived flowlines; (B) - area of divergence between the three DEM-types; and (C) - area where QL1 lidar-derived DEMs resulted in continuous flow paths; there are other similar areas in the watershed.

the Brooker Creek watershed, the three DEMs produced completely different paths through wetland areas (**Figure 4**).

In the more urbanized Cross Bayou Canal/Lake Seminole watershed, there are also areas where the flowlines are in close agreement among all three DEM-types (**Figure 5A**), as well as areas where there is little agreement (**Figure 5B**). In the urban areas, there were several areas where the GM-derived DEM resulted in flowlines that stopped, whereas the QL1 lidar-derived DEMs provided continuity (**Figure 5C**).

Comparison to SWFWMD ground-truth
As indicated previously, the SWFWMD

lidar specification prescribes that all channelized features are captured as either single-line (less than 8' wide) or double-line (greater than 8' wide) drains. The SLDs in the watersheds were buffered to produce polygons and used to clip the flowlines resulting from each of the three DEM-types. The total lengths of the clipped lines were summarized (**Tables 3 and 4**) to indicate the degree of agreement between flowlines and the ground-truth for each DEM-type. In both watersheds, there was over 93% agreement between the QL1 LM-derived flowlines and the SWFWMD ground-truth. The GM-derived DEM performed slightly

better in the Brooker Creek watershed (92.6% agreement) than it did in the Cross Bayou Canal/Lake Seminole watershed (81.4% agreement). Both the QL1- and GM-derived DEMs performed better in both watersheds than the QL2-derived DEM.

Parting comments

The British statistician, George Box, is frequently noted for saying that, "All models are wrong, some are useful" (Box and Draper, 2007, 414). While Box was talking about statistical models, the same could easily be applied to DEMs. We always need to remember that the DEM is a model of the earth, and that

BROOKER CREEK				
		DEM-type		
	SWFWMD ground-truth	USGS/QL2 (LM)	GM	USGS/QL1 (LM)
Linear miles of channelized feature (% of ground-truth)	7.89	5.86 (66.9%)	7.34 (92.6%)	7.41 (93.4%)

Table 3: Comparison of continuous flowlines extracted from lidar-derived DEMs with SWFWMD ground-truth in the Brooker Creek watershed.

CROSS BAYOU CANAL/LAKE SEMINOLE				
		DEM-type		
	SWFWMD ground-truth	USGS/QL2 (LM)	Geiger-mode	USGS/QL1 (LM)
Linear miles of channelized features (% of ground-truth)	56.71	38.59 (52.9%)	47.80 (81.4%)	53.29 (93.6%)

Table 4: Comparison of continuous flowlines extracted from lidar-derived DEMs with SWFWMD ground-truth in the Cross Bayou Canal/Lake Seminole Watershed.

the results are further abstracted as a result of the continuous flow A^t model used to produce the flowlines. With that caveat and with respect to using lidar-derived DEMs for EDH for these two watersheds, therefore, we conclude:

1. Small upper reaches, under the EDH threshold, were equally well resolved in the non-urbanized watershed (Brooker Creek), but in the urban environment (Cross Bayou Canal/Lake Seminole), both LM-derived DEMs resolved significantly more flowlines. This may have resulted from the algorithms used by the lidar providers to decimate the GM lidar. The decimation or smoothing had little effect in the rural terrain, where the LM lidar also produced a smoother DEM. In the urban terrain, however, the LM lidar point clouds were more detailed and provided additional definition for those upper reaches.
2. In terms of total network length and reach-number metrics, each of the DEMs performed well, and the metrics were not significantly different. But in both watersheds, the QL1-derived DEMs produced slightly more reaches and a slightly longer network.
3. Geometric differences that could be attributed to the DEM were most striking when the flowlines were compared to SWFWMD ground-truth. In both watersheds, the QL1-derived DEMs produced a geometric network that more closely resembled the ground-truth. Again, possibly as a result of the decimation algorithm used for the GM lidar, the QL1 advantage was greater in the urban watershed (93.6% vs. 81.4% agreement) than in the rural watershed (93.4% vs. 92.6%).
4. Overall, both the QL1 and GM high-density lidar-derived DEMs

outperformed the lower-density QL2-derived DEM for EDH extraction. Future comparisons between the high-density technologies need to account for GM decimation and other low-level lidar processing differences, such as DEM construction methodologies and hydro-conditioning techniques. **1**



Alvan "AI" Karlin, PhD, CMS-L, GISP is a senior geospatial scientist at Dewberry, formerly from the Southwest Florida Water Management District (SWFWMD), where he

managed all the remote sensing and lidar-related projects in mapping and GIS. With Dewberry, he serves as a consultant on Florida-related lidar, topography, hydrology, and imagery projects, as well as general GIS-related projects. He has a PhD in computational theoretical genetics from Miami University in Ohio. He is vice president of ASPRS, a director of the ASPRS Florida Region, an ASPRS Certified Mapping Scientist-Lidar, and a GIS Certification Institute Professional.

References

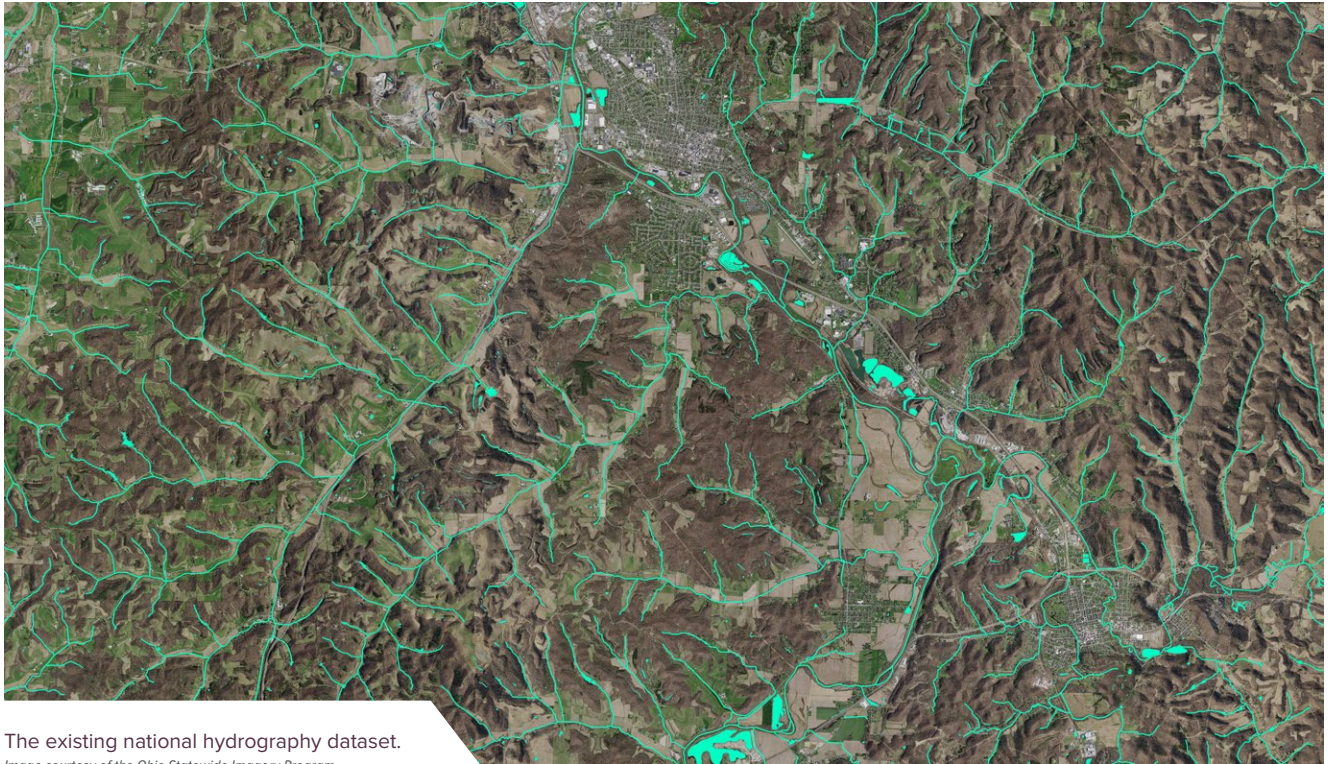
Box, G.E.P. and N. R. Draper, 2007. *Response Surfaces, Mixtures, and Ridge Analyses*, 2nd edition, John Wiley & Sons, Hoboken, New Jersey, 880 pp.

Ehlschlaeger, C. R., 1989. Using the AT search algorithm to develop hydrologic models from digital elevation data, *International Geographic Information Systems (IGIS) Symposium*, 89: 275-281.

Lin, Y-C., S. Jinyuan, S-Y. Shin, Z. Saka, M. Joseph, R. Manish, S. Fei, and A. Habib, 2022. Comparative analysis of multi-platform, multi-resolution, multi-temporal lidar data for forest inventory, *Remote Sensing*, 14: 649-676.

Strahler, A.N., 1952. Dynamic basis of geomorphology, *Geological Society of America Bulletin*, 63: 923-938.

Tarboton, D. G., R. L. Bras, and I. Rodríguez-Iturbe, 1991. On the extraction of channel networks from digital elevation data, *Hydrological Processes*, 5: 81-100.



The existing national hydrography dataset.
Image courtesy of the Ohio Statewide Imagery Program.

Decades of Historic Data Finished

Ohio turns to elevation-derived hydrography

Accurate geospatial data on surface water and drainage is crucial for planning, engineering, and daily operational activities for every county in every state. Nevertheless, Ohio has coped for decades without a full set of timely,

comprehensive geospatial surface water and drainage data. This shortfall has prevented public and private stakeholders, including engineers, farmers, and developers, from understanding current drainage scenarios and engineering effective subsurface drainage solutions. The outdated data has also impacted

the effectiveness of Ohio's water quality programs and the development and construction of numerous county infrastructure projects, all of which rely upon relevant geospatial insights.

Until recently, Ohio's existing drainage information came from the National Hydrography Dataset (NHD)¹, which outlines rivers, streams, canals, lakes, ponds, and other water bodies to generate comprehensive, national hydrography insights. Within the NHD, Ohio's data was based on the digitization of surface water features from 1:24,000 U.S. Geological Survey (USGS) topographic maps created as far back as the 1950s. The accuracy and level of

BY BRIAN STEVENS

¹ usgs.gov/national-hydrography/national-hydrography-dataset



The Ohio Surface Water Model dataset.
Image courtesy of the Ohio Statewide Imagery Program.

detail of these federal maps have been outpaced in recent decades by changing landscapes and advancing mapping and recording technologies. As a result, Ohio's NHD dataset needed an update.

"Our watershed data was outdated," said Jeff Linkous, engineer, Clinton County. "It didn't accurately depict where the true flow of water existed. This was mainly due to changes over time that streams experienced, not only from human development but also from high water and flooding. Our county would benefit from accurate data."

To provide those benefits, Woolpert developed the Ohio Surface Water Model, an initiative owned and managed by the Ohio Geographically Referenced Information Program (OGRIP), which is overseen by the Ohio Department of Administrative Services (ODAS)

Office of Information Technology. The program was designed to replace Ohio's hydrography data with elevation-derived hydrography (EDH). Currently, 11 Ohio counties have led the way by supporting the replacement of the existing hydrography dataset. Without any financial assistance, the counties funded the updates to the surface water and drainage data for their respective localities, knowing that this would meet critical needs. Their decision to put money towards replacing their data was commended by several state legislators and Ohio organizations such as the County Engineers Association of Ohio, the County Commissioners Association of Ohio, The Nature Conservancy in Ohio, and the Ohio Scenic Rivers Association. With widespread support, Woolpert has continued promoting

the creation of EDH data for additional counties. Meanwhile, state agencies and legislators are exploring the best way to expand the effort and partner with the USGS, as was done with the 3D Elevation Program², a USGS initiative created to deliver high-resolution, three-dimensional elevation data of the U.S.

Leveraging 3DEP and 3DHP

Since 1884, USGS has been mapping the nation, delivering critical topographic and hydrographic insights supporting land management and development across the U.S. As a result of crucial advances in mapping technologies, USGS started gathering high-quality topographic data in 2016 for one of its latest efforts: 3DEP, the first national

² usgs.gov/3d-elevation-program

baseline of consistent, high-resolution topographic elevation data. USGS wanted to derive all new hydrography from 3DEP data. This effort started with developing consistent standards and specifications for EDH, which relies on elevation data from lidar or interferometric synthetic aperture radar to generate vector hydrologic networks.

When Woolpert and OGRIP launched the Ohio Surface Water Model for several counties, it leveraged the elevation data available from 3DEP to provide high-resolution hydrographic data for EDH development. Woolpert also relied on the 3D Hydrography Program (3DHP)³, the USGS initiative designed to “significantly improve the level of detail, currency, and content of hydrography data by deriving 3D stream network datasets and watersheds from the high-quality 3D Elevation Program.” Specifically, the Ohio Surface Water Model includes an EDH network generated from and integrated with 3DEP elevation data that is intended for input into 3DHP to provide data accuracy and the attributes needed to model and analyze Ohio’s surface water and coastline as well as better represent stream gradients, channel conditions, water bodies, hydrologic units, hydrologically enhanced elevation, and other surfaces.

“Surface water bodies are very dynamic,” said Neil Tunison, engineer, Warren County. “They change. They drop sediments, and they’re constantly adjusting course. Having this data [updated] on a fairly regular basis will help us with planning.”

Still, Woolpert and OGRIP wanted to take things a step further. Baseline 3DHP data derived from 3DEP lidar for the continental U.S. represents streams

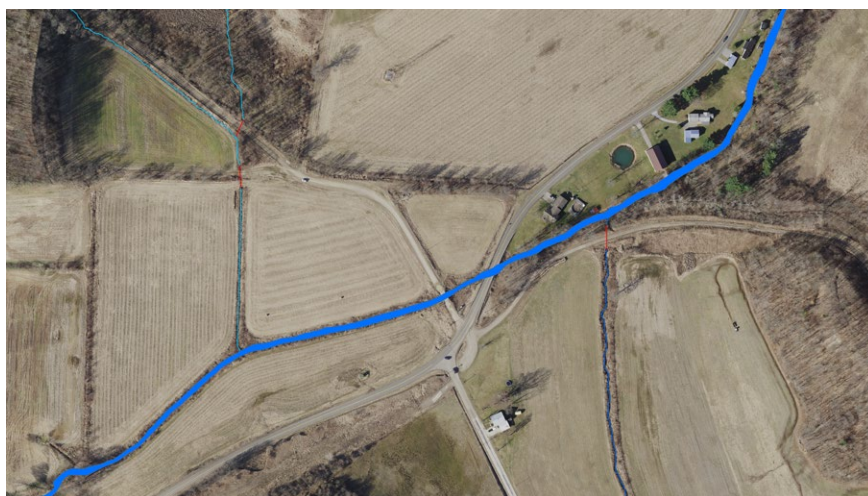
and canals as polygons for features 50 feet and wider and lakes and ponds greater than about ¼ acre. One of the goals of the Ohio Surface Water Model was to ensure the dataset also included ephemeral water when evident on the elevation surface per EDH specifications. Ephemeral water is surface water that flows briefly in direct response to precipitation in the immediate vicinity. Counties, state agencies, and several organizations conveyed their need for Woolpert to collect polygonal data on perennial water for 15-foot or wider streams and rivers, ephemeral flowlines, and lakes and ponds greater than ¼ acre. Once the hydrography was completed for the 11 Ohio counties, contours were generated, which the counties plan to use for a wide range of applications, including preliminary engineering, planning, and economic development. Achieving this would enable Woolpert and OGRIP to capture hydrographic features at a four- to six-times-greater level of drainage detail than is currently available, and core attributes of the hydrography would be identified and defined for all features

gathered. However, achieving this with the Ohio Surface Water Model required innovative technologies.

Exceeding expectation demands exceedingly powerful technology

Woolpert used artificial intelligence (AI) and machine learning (ML) to generate the 3DHP data for the Ohio Surface Water Model, followed by manual verification to increase confidence that the information produced was accurate. These technologies assisted in identifying drainage patterns that affect flooding characteristics, stream flows, and water quality. Traditionally, 3D photogrammetric techniques or heads-up digitization from orthoimagery base-mapping was relied upon to compile hydrography data manually. Although time-consuming and laborious (especially when used for large areas), these techniques successfully identified perennial bodies of water for decades. They fell short, however, in their ability to identify ephemeral water bodies and drainage patterns.

Woolpert needed new technology to gather the desired data as well as



The lidar surface model overlaid with perennial and ephemeral surface water and flowlines. Image courtesy of the Ohio Statewide Imagery Program.

3 usgs.gov/index.php/3DHP



This image showcases the high-resolution complement to existing base mapping data.
Image courtesy of the Ohio Statewide Imagery Program.

new processes to extract hydrography features from the ingested datasets. The new datasets typically included four-band orthoimagery and high-density aerial lidar at a density of eight points per square meter or more. When considering the varied topography across states, counties, and watersheds, no existing manual methods could extract ephemeral drainage effectively or accurately. The solution was AI and ML. Using high-density aerial lidar input consisting of millions or billions of points for a statewide project, AI and ML processes successfully identified ephemeral flowlines as well as small lakes, ponds, rivers, and streams.

The promising features of AI and ML

AI and ML proved to be the best solutions for producing the desired 3DHP enhancements due to their promising capabilities for mapping surface features, especially when

coupled with cloud computing. For example, Woolpert used AI to extract features automatically from aerial lidar and determine the flow direction and definition of specific water bodies. Microsoft Azure Machine Learning Studio was instrumental in Woolpert's effort to develop, deploy, and manage these models effectively and with increased confidence. Additionally, cloud computing enabled Woolpert to store and process the large quantities of remote sensing data essential for mapping large areas. Combined, these technologies improved the precision, efficiency, and scalability of EDH.

Ohio counties ready to benefit

With enhanced EDH ready to be added to Ohio's portion of the 3DHP dataset, the state is finally positioned to experience much-needed advantages.

"Clinton County will benefit from accurate data, as it will help with everything, including culvert and bridge

modeling, road realignment for safety projects, flood plain review, and soil and water maintenance ditches," Linkous said. "It will also help us provide the public with current data that assists with planning and economic development proposals."

Tunison also expressed excitement about the advantages the updated data would provide. He explained that he's eager to incorporate the information with Warren County's structural data, "... to get a better handle on the types of bridges and culverts that need to be replaced and how to handle inlets."

When explaining the infrastructure benefits the updated hydrography will provide, Brett Boothe, engineer, Gallia County, said: "The benefits are very broad. I see opportunities for us to use the data to size our bridges, culverts, catch basins, and any other drainage structures because we're using better data to make decisions. Also, since the county lies along the Ohio River, one of the issues we contend with is flood plains. We have commercial and residential properties within the flood plain. This data will give us a better opportunity to define where those lines are, which makes a big difference when we're talking about our county's economic and residential development. We all know flood-plain insurance is extremely expensive and hinders our growth, so this data will be extremely important from an economic perspective." ■



Brian Stevens is a geospatial program director and vice president at Woolpert. He works out of Woolpert's office in Columbus, Ohio.

BEST PRACTICES

in Evaluating Geospatial Mapping Accuracy according to the New ASPRS Accuracy Standards

Accuracy assessments must take errors in ground control network into account

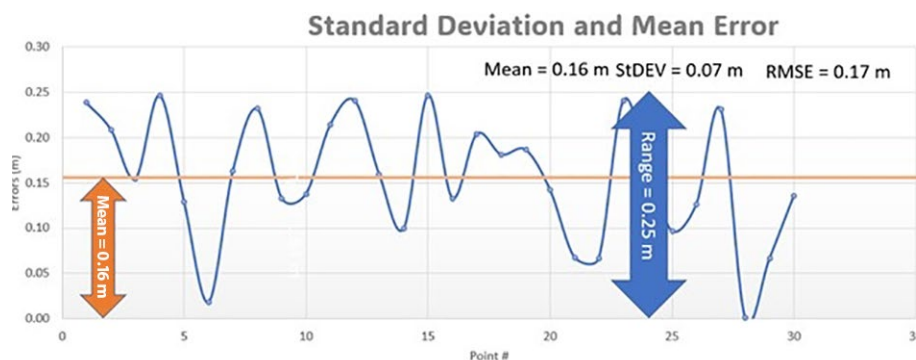


Figure 1: Standard deviation measures the error fluctuation around a mean value of 0.17 m.

This highlight article was inspired by a comment I received from Richard C. Maher, PLS, president of KDM Meridian:

"I attended both of your American Society for Photogrammetry and Remote Sensing (ASPRS) workshops during Geo Week 2024 in Denver. Even after 24 years as a land surveyor, I can still use refreshing on how to explain the basics to my clients and surveyors-in-training. Your in-depth discussion on the difference between the standard deviation and the root mean square error (RMSE) was very appreciated. I also appreciated the concepts of the true datum and the

survey (pseudo) datum you introduced. As one who loves to test and prove that our equipment can rarely do better than the specifications, I'll say unequivocally that surveyors using real-time kinematic (RTK) positioning are far too optimistic about their true accuracy and commonly don't understand apparent relative accuracy due to a fundamental misunderstanding of the error sources different between GPS and conventional measurements. The nature of random error in GPS follows a different stochastic model than conventional instrumentation. If surveyors simply employed the same checking standards and methods you prescribe in the ASPRS

BY GASSIM ABDULLAH

specifications, they'd stop telling me how well their GPS did under a canopy, or how they can get "hundredths." My intention isn't to make their work more difficult but to ensure that our methods are rigorous and reliable... I'm interested in seeing your future appendix that talks about suggested survey accuracies when not provided by surveyors. Due to the importance of these topics to the thousands of practicing surveyors in the nation who could not attend Geo Week, could you please shed light on the concepts you presented in Denver regarding surveying and mapping accuracy and the role of the correct understanding of the datum?"

In my response to this request, I will address these important issues in separate sections.

Standard deviation versus root mean square error (RMSE) estimation

Before we discuss the difference between standard deviation and RMSE as accuracy measures, let us elaborate on the statistical meaning of each.

Standard deviation is a statistical measure of the fluctuation or dispersion of individual errors around the mean value of all the errors in a dataset. **Figure 1** illustrates how the errors fluctuate around a mean error value of 0.16 m. This fluctuation is represented by the standard deviation value, or 0.07 m.

The standard deviation is calculated as the square root of variance by determining each error's deviation relative to the mean as given in the following equation:

$$s_x = \sqrt{\frac{1}{(n-1)} \sum_{i=1}^n (x_i - \bar{x})^2}$$

where:

\bar{x} is the mean error in the specified direction,

x_i is the i^{th} error in the specified direction,

n is the number of checkpoints tested,

i is an integer ranging from 1 to n .

RMSE is the square root of the average of the set of squared differences between dataset coordinate values and coordinate values from an independent source of higher accuracy for identical points. It is obvious from this definition that RMSE differs from standard deviation by the magnitude of the mean error existing in the data. This becomes clear from

the difference between the previous equation, defining the standard deviation, and the following RMSE:

$$RMSE_x = \sqrt{\frac{1}{n} \sum_{i=1}^n (x_{i(\text{map})} - x_{i(\text{surveyed})})^2}$$

where:

$x_{i(\text{map})}$ is the coordinate in the specified direction of the i^{th} checkpoint in the dataset,

$x_{i(\text{surveyed})}$ is the coordinate in the specified direction of the i^{th} checkpoint in the independent source of higher accuracy,

n is the number of checkpoints tested,

i is an integer ranging from 1 to n .

When RMSE is computed, we do not subtract the mean checkpoint error, so RMSE represents the full spectrum of the error found in a checkpoint, including the mean error, whereas, in computing the standard deviation, we subtract the mean error from every checkpoint error, making it a measure of the fluctuation of individual errors around the mean value of all the errors. This RMSE characteristic makes it useful in flagging biases in data, as it provides an early warning system for the technician that the standard deviation fails to do.

Biases and systematic errors in data

Now we understand the difference between the standard deviation and RMSE, let us see how such favoring of the RMSE helps the geospatial mapping production process and validation of the accuracy of its products. Geospatial mapping products are subject to systematic errors or biases from a variety of sources. These biases can be caused by things like using the wrong version of a datum during the product production process, or using the wrong instrument height for the tripod during the survey computations for the ground control points or the checkpoints. There are other sources of biases that can be introduced during the production process. For instance, using the wrong elevation values in digital elevation data can result in biases during the orthorectification process, and using the wrong camera parameters (such as focal length) or the wrong lens distortion model can lead to biases in the final mapping product.

Systematic error can cause the product to fall below acceptable project accuracy levels. Thankfully, provided the

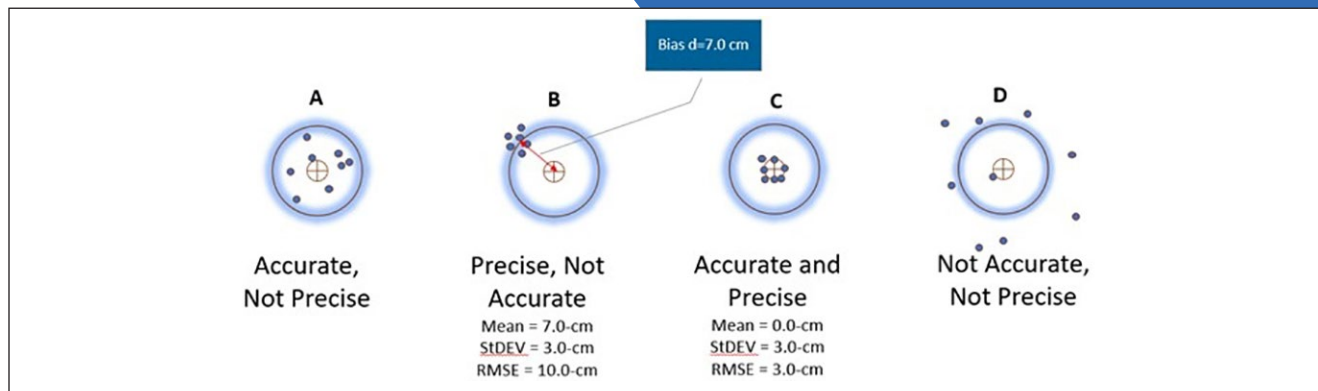


Figure 2: Scoreboards for four archers with varied aiming skills.

appropriate methodologies are applied, systematic error can be identified, modeled, and removed from the data. This is not the case with random error: even if we discover it, we cannot eliminate it. However, we can minimize random error magnitude through adherence to a stringent production process, adopting sound quality control practices, or the use of more accurate instruments. To illustrate systematic errors or biases in data, we will evaluate the scoreboards of four archers who vary in their aiming skills, illustrated in **Figure 2**.

For Board A, the archer landed the arrows around the bullseye, but the shots are scattered spatially around the center point. By contrast, Board B reflects good spatial clustering, but the shots are clustered around a point far away from the bullseye. Board C is what one wants accuracy to be, with all shots clustered at the aimed spot. Board D demonstrates extremely undesirable results, possessing neither good clustering, nor good aiming.

When we measure accuracy, results like boards B and C are the most desirable. Board C should be preferred, as it represents clean results: All shots are at the bullseye. We can describe archer C as “accurate and precise.” Although archer B’s results lack good aim, the shots are clustered well. We describe archer B as “precise but not accurate.” Even though archer B is not accurate, why are these results still acceptable? Examine the scoreboard for archer B again: if we shift the locations of all the clustered arrows by a fixed distance d , or 7.0 cm, the results will match the results from archer C. This distance d or 7.0 cm represents the systematic error; once it is corrected, the final accuracy will be satisfactory.

But why did such a precise archer miss the bullseye to begin with? We must consider what may have taken place at the

archery range to cause archer B to miss. Perhaps the archer was using a sight scope hooked to the archer bow. Having all the arrows land in a tight cluster away from the bullseye is a strong indication of a mechanical failure of the sight scope that caused the arrows to go to the wrong place. Once archer B’s sight scope is properly calibrated, the archer scoreboard in the second archery session will look just like archer C’s board. The same logic can be applied to geospatial products such as lidar point clouds or orthoimagery. That is why it is crucial to use accurate checkpoints when verifying product accuracy. These checkpoints will help us quantify any existing systematic errors, allowing us to remove this error from the data in the same way that properly calibrating archer B’s sight scope corrects the archer future shots.

True datum versus surveying pseudo datum

When we conduct field surveying, we are trying to determine terrain positions and shapes with reference to a specific geodetic datum. According to the U.S. National Geodetic Survey (NGS), a geodetic datum is defined as “an abstract coordinate system with a reference surface (such as sea level, as a vertical datum) that serves to provide known locations to begin surveys and create maps.” Because our surveying techniques, and therefore our mapping techniques, are not perfect, our surveying techniques provide only approximate positions that put us close to the true, datum-derived positions (**Figure 3**). When we use an inaccurately surveyed network to control another process such as aerial triangulation, we are fitting the aerial triangulation solution to an observed datum. The degree of approximation depends on the accuracy of the surveying technique or technology employed in that survey. The RTK

field surveying technique, for example, can produce positions that are accurate to 2 cm horizontally and perhaps 2-3 cm vertically. The differential leveling technique used to determine height can produce elevations that are accurate to the sub-centimeter. The lesson to learn here is that our surveying techniques, no matter how accurate, do not represent the true datum—but they can get us close to it.

Surveying and survey (pseudo) datum

When we task surveyors to survey the ground control network with reference to a certain datum, usually a true datum such as NAD83 or WGS84, they can determine the positions of the control network to that datum only as close as the surveying techniques allow. In other words, the coordinates used to control the mapping process represent an observed or survey datum that forms a pseudo datum, green mesh in **Figure 3**, but not the original intended or true datum represented by the solid green in **Figure 3**. For example, if we are trying to determine point coordinates in NAD83(2011), the surveyed coordinates used in aerial triangulation or lidar calibration represent a datum that is close to NAD83(2011) but not exactly NAD83(2011), due to the inaccuracy in our surveying techniques. That inaccurate survey represents a survey datum. Besides the inaccuracy in the surveying techniques, another layer of errors (i.e., distortion) could be added to the surveyed coordinates when we convert geographic positions (in latitude

and longitude) to projected coordinates or grid coordinates, such as state plane coordinate systems.

Mapping to the mapping datum

Any mapping process we conduct today inherits two modeling errors that influence product accuracy. The first modeling error is caused by the inaccuracy of the internal geometric determination during the aerial triangulation, or the boresight calibration in the case of lidar processing. The second modeling error is introduced by the auxiliary systems, such as GNSS and IMU, and has inherent errors caused by the survey datum. Therefore, when we use mapping products to extract location information, we are determining these locations with reference to the survey or pseudo datum and not the true intended datum. The point coordinates for NAD83(2011) are determined not according to the survey datum of the ground control network but through a new reality of mapping datum. The mapping datum, represented with the blue mesh in **Figure 3**, inherits the errors of the survey datum, which were caused by the inaccuracy of our surveying techniques and the errors caused by our mapping processes and techniques.

Correct approach to accuracy computation

To reference the accuracy of determining a mapped object location within a mapping product with reference to the original intended datum such as NAD83(2011), we need to examine the layers of error that were introduced during the ground surveying and mapping processes (**Figure 3**).

Currently, users of geospatial data express product accuracy based on the agreement or disagreement of the tested product with respect to the surveyed checkpoints, ignoring checkpoint or ground control errors that have resulted from inaccurate surveying techniques. In other words, users consider the surveyed points to be free of error. The following section details how errors are propagated into the mapping product when we are trying to determine the location of a ground point “A”. Let us introduce the following terms—refer to **Figure 3** for localizing such error terms:

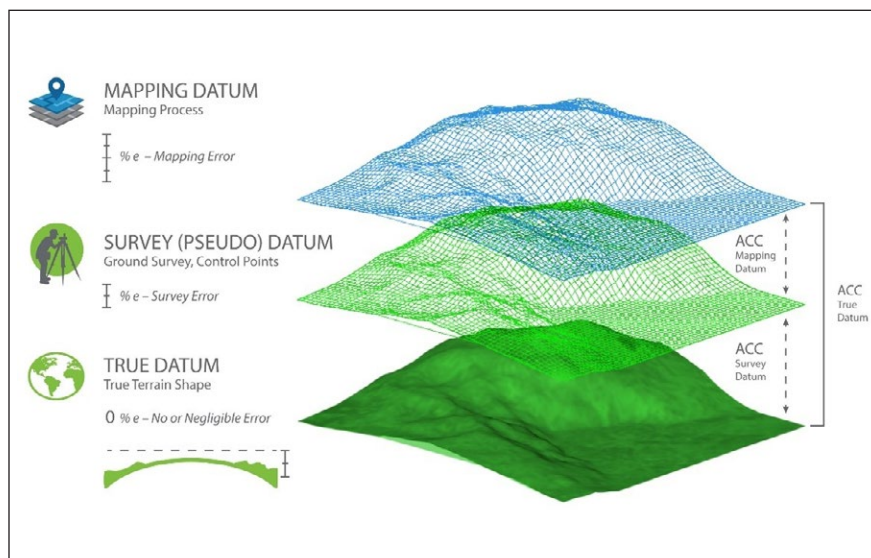


Figure 3: Datums and error propagation in geospatial data.

$ACC_{SurveyDatum}$ equals the accuracy in determining the survey datum, generated when realizing the intended or true datum through surveying techniques. In other words, it represents the errors in the surveyed checkpoints. Due to this inaccuracy, the point will be located at location A'' (Figure 4).

$ACC_{MappingDatum}$ equals the accuracy of determining the mapping datum, or the errors introduced during the mapping process, with reference to the already inaccurate survey datum represented by the surveyed checkpoints. In other words, it is the fit of the aerial triangulation (for imagery) or the bore-sight/calibration (for lidar) to the surveyed ground control points represented as the survey datum. This accuracy is measured using the surveyed checkpoints during the product accuracy verification process. Due to this inaccuracy, the point will be located at location A''' (Figure 4).

$ACC_{TrueDatum}$ equals the accuracy of the mapping product with reference to the true datum, for example NAD83(2011). The point location A' (Figure 4) is considered the most accurate location determined with reference to the true datum.

Using the above definitions, the correct product accuracy should be modeled using error propagation principles according to the following formula:

$$ACC_{TrueDatum} = \sqrt{ACC_{MappingDatum}^2 + ACC_{SurveyDatum}^2} \quad \text{EQ1}$$

However, according to our current practices, product accuracy is computed according to the following formula, ignoring errors in the surveying techniques:

$$ACC_{TrueDatum} = ACC_{MappingDatum} \quad \text{EQ2}$$

More details and examples on the suggested approach can be found in my published article¹ on the topic and Edition 2 of the *ASPRS Positional Accuracy Standards for Digital Geospatial Data*².

The new approach to computing map accuracy

According to this new approach to computing map accuracy and since we are dealing with three-dimensional error components, we would need to employ vector algebra to accurately compute the cumulative error.

1 Abdullah, Q., 2020. Rethinking error estimations in geospatial data: the correct way to determine product accuracy, *Photogrammetric Engineering & Remote Sensing*, 86 (7): 397-403, July 2020.
2 publicdocuments.asprs.org/PositionalAccuracyStd-Ed2-V1

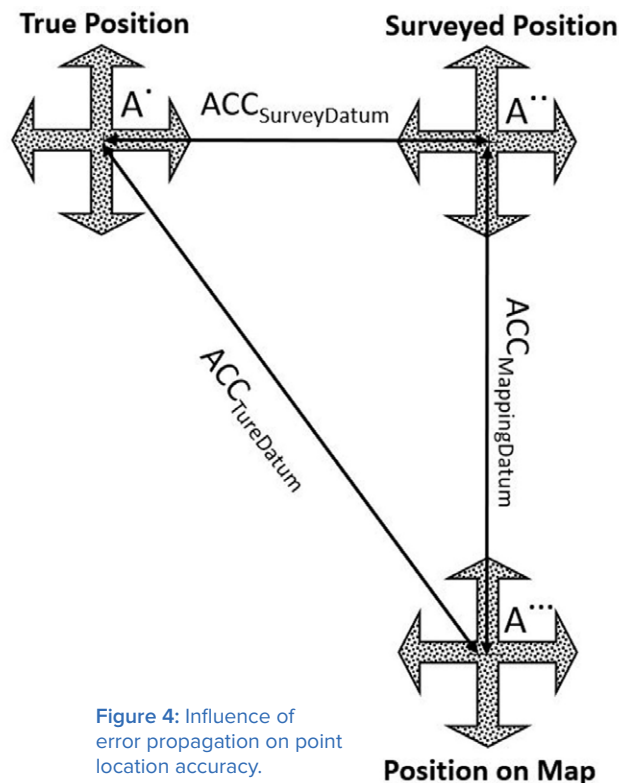


Figure 4: Influence of error propagation on point location accuracy.

Computing horizontal accuracy

To compute the horizontal accuracy for a two-dimensional map, as with orthorectified imagery, we will ignore the error component of the height survey. In other words, we will use the error component from easting and northing only. We will also assume that the accuracy of determining the X coordinates (or eastings) is equal to the accuracy of determining the Y coordinates (or northings). Using error propagation principles and Euclidean vectors in Figures 4 and 5, we can derive the following values for product horizontal accuracy:

$$AccX_{TrueDatum} = \sqrt{AccX_{MappingDatum}^2 + AccX_{SurveyDatum}^2} \quad \text{EQ3}$$

$$AccY_{TrueDatum} = \sqrt{AccY_{MappingDatum}^2 + AccY_{SurveyDatum}^2} \quad \text{EQ4}$$

$$AccXY_{TrueDatum} = \sqrt{AccX_{TrueDatum}^2 + AccY_{TrueDatum}^2} \quad \text{EQ5}$$

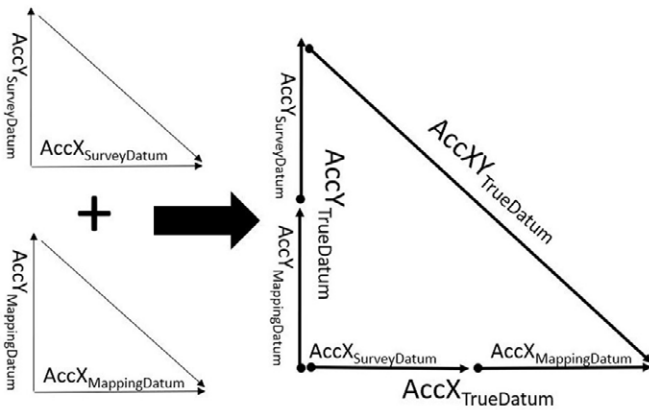


Figure 5: Vector representations of error components.

As an example, when modeling horizontal product accuracy according to the above formulas, let us assume the following:

- We are evaluating the horizontal accuracy for orthoimagery using independent checkpoints.
- The control survey report states that the survey for the checkpoints, which was conducted using RTK techniques, resulted in accuracy of $RMSE_{XorY}$ equal to 2 cm.
- When the checkpoints were used to verify the horizontal accuracy of the orthoimagery, the result was an accuracy of $RMSE_{XorY}$ equal to 3 cm.

Thus, from equations 3, 4 and 5:

$$AccX_{TrueDatum} = \sqrt{3^2 + 2^2} = 3.61\text{cm} \quad \text{EQ3}$$

$$AccY_{TrueDatum} = \sqrt{3^2 + 2^2} = 3.61\text{cm} \quad \text{EQ4}$$

$$AccXY_{TrueDatum} = \sqrt{3.61\text{cm}^2 + 3.61\text{cm}^2} = 5.1\text{cm} \quad \text{EQ5}$$

The value of 5.1 cm is the true accuracy of the product versus the following value of 4.24 cm used commonly today that ignores the errors introduced during the ground surveying process:

$$AccXY_{TrueDatum} = \sqrt{3\text{cm}^2 + 3\text{cm}^2} = 4.24\text{cm} \quad \text{EQ5}$$

Computing vertical accuracy

Similarly, for vertical accuracy determination of elevation data derived from lidar or photogrammetric methods, we need to consider the error in the surveyed elevation as an important component. Using error propagation principles and the Euclidean vectors of **Figure 6**, we can derive the following value for vertical product accuracy:

$$AccZ_{TrueDatum} = \sqrt{AccZ_{MappingDatum}^2 + AccZ_{SurveyDatum}^2} \quad \text{EQ6}$$

As an example, when modeling vertical product accuracy according to the above formulas, let us assume that:

- We are evaluating the vertical accuracy for a mobile lidar dataset using independent checkpoints.
- The control survey report states that the survey of the checkpoints, which was conducted using RTK techniques, resulted in an accuracy of $RMSE_Z$ equal to 3 cm.
- When the checkpoints were used to verify the vertical accuracy of the lidar data, the results was an accuracy of $RMSE_Z$ equal to 1 cm.

Thus, from equation 6:

$$AccZ_{TrueDatum} = \sqrt{1^2 + 3^2} = 3.61\text{cm} \quad \text{EQ6}$$

The value of 3.16 cm is the true vertical accuracy of the lidar dataset, versus the value of 1 cm derived by the mapping technique used commonly that ignores the errors introduced during the ground surveying process.

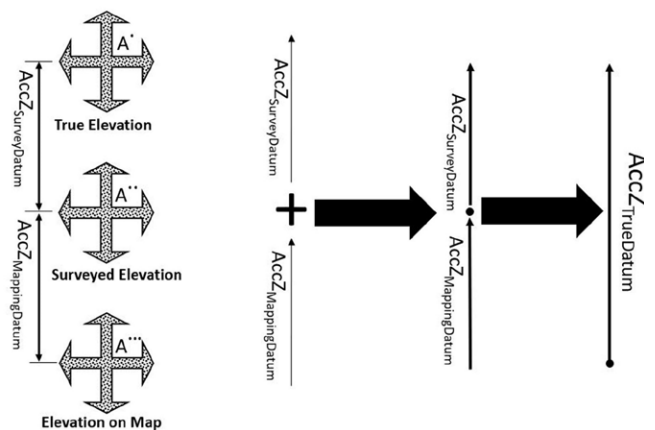


Figure 6: Influence of error propagation on point elevation accuracy.

The role of RMSE in revealing biases in data

Now, let's see how we are going to assess the accuracy computations, and whether we can spot problems in the data. We assume a scenario in which systematic error was introduced into a lidar dataset during the product generation. Say a technician used the wrong version of the geoid model when converting the ellipsoidal heights of the point cloud to orthometric heights, which caused a systematic error or bias of 0.16 m in the computed elevation of the processed lidar point cloud. **Table 1** lists the results of the accuracy assessment where 30 checkpoints are used for the test.

To analyze the accuracy results, first look at the error mean value in **Table 1**. We clearly notice that the mean error is high as compared to the RMSE and the standard deviation. The *ASPRS Positional Accuracy Standards for Digital Geospatial Data* advise that a mean error value that is more than 25% of the RMSE is an indication of biases in the data that need to be dealt with and resolved before accepting and delivering the lidar data. So, we will focus on the results in **Table 1** for further analysis. A high mean error value is a good indication that biases are present in the data, but we need to further investigate how high the mean value is compared to RMSE and standard deviation. Slight differences between these statistical measures' values are acceptable. Looking at the results of **Table 1**, the mean error reaches 91% of the RMSE value, which is not acceptable according to the ASPRS standards.

Table 1: Accuracy assessment for a biased dataset.

Point #	Surveyed Coordinates			Lidar	Error Values (m)
	Easting (m)	Northing (m)	Elevation (m)	Elevation (m)	
CP_1	746093.605	97840.580	332.708	332.469	0.239
CP_2	746084.481	97875.486	333.856	333.646	0.209
CP_3	746076.993	97906.423	334.791	334.636	0.155
CP_4	746069.043	97934.869	335.829	335.582	0.247
CP_5	746059.191	97968.525	336.837	336.708	0.129
CP_6	746051.284	97996.814	337.671	337.652	0.018
CP_7	746044.837	98025.039	338.717	338.553	0.163
CP_8	746036.494	98055.805	339.823	339.591	0.232
CP_9	746027.369	98082.550	340.646	340.513	0.134
CP_10	746019.781	98112.192	341.636	341.498	0.138
CP_11	746012.222	98144.373	342.792	342.577	0.215
CP_12	746006.094	98171.008	343.667	343.426	0.241
CP_13	745998.080	98196.380	344.486	344.326	0.160
CP_14	745987.766	98231.319	345.597	345.498	0.100
CP_15	745939.681	98221.349	347.036	346.789	0.247
CP_16	745950.670	98190.848	345.788	345.655	0.133
CP_17	745956.968	98166.660	344.999	344.795	0.204
CP_18	745966.818	98133.845	343.825	343.644	0.182
CP_19	745977.417	98100.689	342.676	342.489	0.187
CP_20	745986.146	98071.263	341.594	341.451	0.143
CP_21	745994.431	98044.637	340.573	340.505	0.068
CP_22	746003.437	98011.200	339.403	339.336	0.067
CP_23	746013.675	97977.662	338.426	338.185	0.241
CP_24	746020.633	97952.708	337.451	337.282	0.169
CP_25	746029.450	97922.620	336.316	336.219	0.097
CP_26	746037.820	97896.313	335.422	335.295	0.127
CP_27	746073.182	98205.333	343.418	343.186	0.231
CP_28	746137.202	98304.228	344.254	344.253	0.001
CP_29	746046.203	97866.550	334.320	334.253	0.067
CP_30	746056.297	97832.573	333.199	333.063	0.136
Number of Checkpoints					30
Minimum Error					0.001
Maximum Error					0.247
Mean Error					0.156
Median Error					0.157
Standard Deviation					0.069
RMSE					0.170
Horizontal Positional Accuracy (E & N)					N/A
Vertical Positional Accuracy					0.170
3D Positional Accuracy					N/A

Table 2: Accuracy assessment after bias removal.

Point #	Surveyed Coordinates			Biased Lidar	Unbiased Lidar	Unbiased Error Values (m)
	Easting (m)	Northing (m)	Elevation (m)	Elevation (m)	Elevation (m)	
CP_1	746093.605	97840.580	332.708	332.469	332.625	0.083
CP_2	746084.481	97875.486	333.856	333.646	333.802	0.053
CP_3	746076.993	97906.423	334.791	334.636	334.792	-0.001
CP_4	746069.043	97934.869	335.829	335.582	335.738	0.091
CP_5	746059.191	97968.525	336.837	336.708	336.864	-0.027
CP_6	746051.284	97996.814	337.671	337.652	337.808	-0.138
CP_7	746044.837	98025.039	338.717	338.553	338.709	0.007
CP_8	746036.494	98055.805	339.823	339.591	339.747	0.076
CP_9	746027.369	98082.550	340.646	340.513	340.669	-0.022
CP_10	746019.781	98112.192	341.636	341.498	341.654	-0.018
CP_11	746012.222	98144.373	342.792	342.577	342.733	0.059
CP_12	746006.094	98171.008	343.667	343.426	343.582	0.085
CP_13	745998.080	98196.380	344.486	344.326	344.482	0.004
CP_14	745987.766	98231.319	345.597	345.498	345.654	-0.056
CP_15	745939.681	98221.349	347.036	346.789	346.945	0.091
CP_16	745950.670	98190.848	345.788	345.655	345.811	-0.023
CP_17	745956.968	98166.660	344.999	344.795	344.951	0.048
CP_18	745966.818	98133.845	343.825	343.644	343.800	0.026
CP_19	745977.417	98100.689	342.676	342.489	342.645	0.031
CP_20	745986.146	98071.263	341.594	341.451	341.607	-0.013
CP_21	745994.431	98044.637	340.573	340.505	340.661	-0.088
CP_22	746003.437	98011.200	339.403	339.336	339.492	-0.089
CP_23	746013.675	97977.662	338.426	338.185	338.341	0.085
CP_24	746020.633	97952.708	337.451	337.282	337.438	0.013
CP_25	746029.450	97922.620	336.316	336.219	336.375	-0.059
CP_26	746037.820	97896.313	335.422	335.295	335.451	-0.029
CP_27	746073.182	98205.333	343.418	343.186	343.342	0.075
CP_28	746137.202	98304.228	344.254	344.253	344.409	-0.155
CP_29	746046.203	97866.550	334.320	334.253	334.409	-0.089
CP_30	746056.297	97832.573	333.199	333.063	333.219	-0.020
Number of Checkpoints						30
Minimum Error						-0.155
Maximum Error						0.091
Mean Error						0.000
Median Error						0.001
Standard Deviation						0.069
RMSE						0.067
Horizontal Positional Accuracy (E & N)						N/A
Vertical Positional Accuracy						0.067
3D Positional Accuracy						N/A

Table 3: Best predicted accuracies for surveying techniques¹.

Survey Methodology	Best Predicted Accuracy Values (mm)		
	Horizontal	Vertical	3D
Adjusted Closed Loop – Digital Levelling		5	
Real Time Network Following Section C – Recommended Procedures	10	16	19
Real Time PPP After Convergence Following Section D – Recommended Procedures	15	24	28
Real Time Kinematic (RTK) Single Measurement Following Section B – Recommended Procedures	20	32	38
Closed Conventional Traverse Following Section E – Recommended Procedures	25	40	47
Real Time PPP After Convergence, Single Measurement	20	50	54

¹ Addendum II of the *ASPRS Positional Accuracy Standards for Digital Geospatial Data*, Edition 2, V2.

We also need to compare the RMSE to the standard deviation. Note that they are 0.170 m and 0.069 m, respectively. An RMSE value more than twice the standard deviation is a strong indication that biases may be present in the data. Remember that, in the absence of systematic errors, i.e., biases, the RMSE and the standard deviation should be equal. This conclusion is also supported by the fact that the mean is twice as high as the standard deviation.

Now that we have concluded that the data has biases in it, let us see how we will remove these without reproducing the product from scratch. For lidar data, we will need to raise or lower the computed heights for the point cloud by the amount of the bias—in this case, 0.16 m. Since the mean is a positive value, and the values in the “Error Values” column were computed by subtracting the lidar elevation from the checkpoint elevation, or:

$$\text{Error} = \text{Surveyed Elevation} - \text{Lidar Elevation}$$

We can then conclude that the terrain elevation as determined from the lidar data is lower than that measured by the surveyed checkpoints. Thus, we need to raise the lidar elevations by 0.16 m. **Table 2** illustrates the bias treatment we introduced above, where the modified accuracy assessment values are listed in column “Unbiased Error Values.” All we did here was raise, or z-bump, the elevations of the point cloud by the amount of the bias, 0.16 m.

“I call on all professional societies, such as NSPS, ASPRS, ASCE, TRB, to lead a campaign to educate their members on the importance of this issue, and on all state agencies—which are tasked with the professional certification of surveyors, mappers, and engineers—and NCEES to revise their certification testing materials to include topics raised in this article.”

Similarly, if such an analysis were conducted to investigate the horizontal positional accuracy of an orthoimage, all we would need to do is modify the coordinates of the tile’s header by the amount of the calculated biases without the need to reproduce the orthoimages. It is worth mentioning that removing the bias based on the “mean” value will not necessarily reduce the value of the RMSE by the same amount, as the degree of improvement in the recalculated RMSE

value depends on the value of the standard deviation. For datasets with low standard deviation value and low rates of fluctuation, removal of the biases will improve the RMSE by a more significant degree. With the data cleaned from the bias effect, all conditions for good accuracy results are satisfied and clearly presented in **Table 2**. The mean error is zero as the bias was removed, and the standard deviation and the RMSE values are equal.

The new approach and challenges for users

As we introduced the new approach in modeling products' accuracy, I was surprised by the following findings.

Survey accuracy and surveyors' awareness

As expressed in equation 1, the new approach requires the user to enter an absolute accuracy figure for the surveyed local network. To my surprise, I found most surveyors I spoke with were either not aware of where to find this accuracy figure in the instrument processing report, or blindly trusted numbers in reports where the accuracy is presented as a quality measure that does not relate to the absolute accuracy as called for by the new approach. I reviewed several processing reports from some surveying instruments where such a figure approaches zero, for example 0.002 m.

Surveying instruments manufacturers and survey accuracy

To follow up on this, the ASPRS accuracy standard working group contacted several manufacturers of surveying instruments, but we did not get straight answers to our request as most manufacturers do not report such absolute accuracy figures. To me, it seems that a reported accuracy figure of close to zero represents a precision measure from multiple survey sessions of the same point. Users of these instruments need to know that all current surveying instruments, no matter how accurate, cannot produce a surveying accuracy of 0.002 m.

Surveyors' and mappers' power

Surveyors and other users of these instruments need to unite and exert their efforts with the surveying equipment manufacturers to provide access to the absolute accuracy of the network survey. Without it, we cannot comply with the accuracy assessment method dictated by the new ASPRS standards. For the time being, and until manufacturers provide us with this accuracy, **Table 3**—which we included in the forthcoming version of the *ASPRS Positional Accuracy*

Standards for Digital Geospatial Data—can be used for the default accuracy values in situations where the survey accuracy is not available or known.

The need to revise the professional practice certification programs

The issues raised in this article are a clear indication of the lack of awareness among professionals about the very issue impacting basic surveying and mapping practices. I call on all professional societies such as NSPS, ASPRS, ASCE, TRB, and others to lead an awareness campaign to educate their members on the importance of this issue. The time is right to start this campaign as we head toward an entire National Spatial Reference System (NSRS) modernization program, to which NOAA and NGS are leading us. The new North American Terrestrial Reference Frame of 2022 (NATRF2022) and the North American-Pacific Geopotential Datum of 2022 (NAPGD2022) will offer more accurate and evolving horizontal and vertical datums, which makes the issues raised in this article even more crucial to the success of our business. Similarly, I put forward a call to all state agencies—which are tasked with the professional certification of surveyors, mappers, and engineers—and NCEES to revise their certification testing materials to include topics raised in this article. Without doing this, we risk the health, safety, and welfare of the public. ■

Note: This article is running in both *Photogrammetric Engineering & Remote Sensing* and *LIDAR Magazine*.



Woolpert Vice President and Chief Scientist **Qassim Abdullah, PhD, PLS, CP**, has more than 45 years of combined industrial, R&D, and academic experience in analytical photogrammetry, digital remote sensing, and civil and surveying engineering. When he's not presenting at geospatial conferences around the world, Abdullah teaches photogrammetry and remote sensing courses at the University of Maryland and Penn State, authors a monthly column for the ASPRS journal *Photogrammetric Engineering & Remote Sensing*, sits on NOAA's Hydrographic Services Review Panel, and mentors R&D activities within Woolpert and around the world.

Nayegandhi, continued from page 48
Bathymetry Technical Center of Expertise (JALBTCX), and research universities, such as Oregon State University.

TPU considers the random (not systematic) errors associated with each lidar measurement and the fact that each lidar measurement is an estimate with an associated uncertainty. The uncertainty is a combination of multiple factors, including but not limited to timing errors (GPS), and electrical and mechanical positioning errors (IMU). In the case of aerial lidar, laser ranging errors can be caused by scan angles, beam divergence, flying height, size of the laser footprint as the beam interacts with the ground and objects above the ground, as well as local environmental and/or atmospheric conditions. Any errors in lever-arm offsets and boresight calculations should be included in TPU calculations based on information derived from calibration tests. TPU models comprising Total Vertical Uncertainty (TVU) and Total Horizontal Uncertainty (THU) components are already widely used for acoustic survey systems, such as multi-beam echosounders, and can be easily extended to both topobathymetric and topographic lidar surveys.

The case for adding TPU to aerial topographic lidar

There are three logical arguments for including either a combined TPU or two separate measurements (THU and TVU) to the LAS specification:

1. Adding either would provide additional information to the end-user regarding each lidar measurement. In the current LAS specification (LAS 1.4 - R15)⁴, it is assumed that,

barring systematic errors which should have been removed from the dataset, each measurement has the same precision. While attributes associated with each pulse, such as “Scan Angle Rank” are useful, there is no error associated with each to help the end-user assess the mechanical/optical accuracy. Adding TPU (or THU/TVU) would provide the end-user with information to help assess the non-systematic errors in the measurements.

2. Specifying either TPU or THU/TVU to the LAS file would be relatively simple and cost-effective. As Point Data Record (PDR) formats 1-5 are being retired, other relevant fields such as GPS time are already required, and there are currently unused “ASPRS reserved” and/or “User Definable” values, so specifying TPU (or THU and TVU) would be relatively simple in a new PDR format.
3. TPU offers a consistent way to measure the uncertainty of each lidar-derived XYZ location and incorporates uncertainties from various sources that contribute towards the errors for each measurement as described above.

The case against adding TPU to terrestrial aerial lidar

The arguments against adding TPU or THU/TVU to the LAS specification include:


1. There is no outcry in the end-user community for TPU to be included. To the end-user, TPU is still an academic/research endeavor that brings no real monetary value to the data, especially if adding it will incur additional cost. The end-user is more concerned with absolute accuracy and positioning and how

different materials and/or terrains affect that accuracy.

2. As currently proposed, TPU (THU and TVU) would be a function of testing and reporting by manufacturers, rather than *in situ* testing. This could potentially lead to a manufacturer’s “arms race”, for better or worse, to report ever more favorable TPU measurements. While this may improve the overall measurement assessment, it will be dependent on some independent verification, which may, in turn, add costs to the instruments.

Parting thoughts and recommendations

Even though there is no end-user demand to include propagated uncertainty in the LAS specification, the benefits of doing so may outweigh the disadvantages. Having more information regarding the accuracy of the lidar product can only be beneficial to the community. However, safeguarding the integrity of the information with independently verifiable methods ensures that the information is truly useful. Doing so means there will likely be additional pre-mission calibration or testing, which could result in additional cost to the end-user.

We welcome your comments on this topic, and remember, you can also participate in and leave comments with the ASPRS LAS Working Group. 

Amar Nayegandhi, Senior Vice President, Dewberry, leads the firm’s geospatial and technology services team and technology solutions market segment.



Al Karlin, Senior Geospatial Scientist, Dewberry, serves as a consultant on Florida-related lidar, topography, hydrology, and imagery projects.

⁴ asprs.org/wp-content/uploads/2019/07/LAS_1_4_r15.pdf



The case for (and against) propagated uncertainty in aerial topographic lidar

There is a strong case for adding Total Propagated Uncertainty to the LAS specification, but it would almost certainly increase cost.

The Geo Week 2024 conference provided many opportunities for lidar professionals to gather, exchange ideas, and explore new technologies. Since one of the participating organizations was the American Society for Photogrammetry and Remote Sensing (ASPRS), the lidar community enjoyed additional opportunities to share ideas pertaining to the newly released Edition 2 of the *ASPRS Positional Accuracy Standards for Geospatial Data*¹ and the soon-to-be-released ASPRS LAS 1.5 specification. Those who have participated in the ASPRS Lidar Division and its LAS Working Group are well aware that one of the hottest and more contested topics over the past few meetings has been the addition of “propagated uncertainty” to the LAS specification².

One of the most significant new features in *ASPRS Positional Accuracy Standards for Digital Geographic Data, Edition 2*³ is the reference to including the uncertainty in Global Positioning System (GPS)/Global Navigation Satellite System (GNSS) positions when

determining the absolute accuracy of lidar surveys (i.e. considering the accuracy of surveyed checkpoints when computing the accuracy of the final product). This same philosophy can be extended to include the measured variability of the lidar positioning components, the mechanical/optical components producing the lidar pulse, the inertial measurement unit (IMU), and the on-board and external GPS (Figure 1). As these uncertainty values would be unique for each pulse, the question becomes: should uncertainty values be incorporated into the LAS (1.6? 2.0?) specification?

While this may seem like a new approach to assessing the overall positional accuracy of each lidar pulse, it is certainly (pun intended) not a new idea. In the undersea world of sonar bathymetry, especially in water too deep to obtain independent survey checkpoints, the Total Propagated Uncertainty (TPU) has been the standard of the National Oceanic and Atmospheric Administration (NOAA) and the International Hydrographic Organization (IHO) for assessing positional accuracy. By convention, TPU is expressed as a combination of Total Horizontal Uncertainty (THU) and Total Vertical Uncertainty (TVU). Moreover, TPU has been a research topic in topobathymetric lidar for several years with several high-profile agencies, including NOAA, the U.S. Army Corps of Engineers (USACE), the Joint Airborne Lidar

continued on page 47

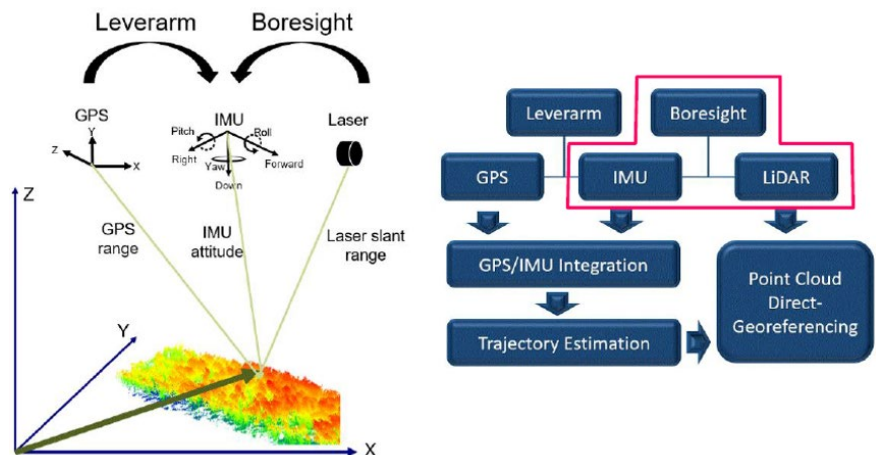


Figure 1: The use of GPS, IMU, and laser ranging measurements to create a directly georeferenced point cloud. Lever-arm offsets and boresight measurements also contribute to the overall accuracy of the point cloud.

Image credit: DEM Users Manual, 3rd edition — Maune, D.F. and A. Nayegandhi (eds.), 2018. Digital Elevation Model Technologies and Applications: The DEM Users Manual, 3rd edition, American Society for Photogrammetry and Remote Sensing, Bethesda, Maryland, 652 pp, p228.

1 asprs.org/visions-to-the-asprs-positional-accuracy-standards-for-geospatial-data-2023
 2 Readers interested in joining the LAS Working Group, which is open to the public, can create a free ASPRS account at community.asprs.org/home.
 3 publicdocuments.asprs.org/PositionalAccuracyStd-Ed2-V1



STONEX
U.S.A.

X70 GO

X⚡WHIZZ MODE

STATIC & DYNAMIC
TOGETHER



THE NEW ERA OF HYBRID SCANNING

www.stonexamerica.com

Stonex USA | 54 Regional Dr. | Concord 03301 - New Hampshire

For a Stonex dealer near you contact us:
Phone: 603-715-5771 | sales@stonexamerica.com

LIDAR USA 
3D MAPPING SOLUTIONS



Surveyor 120 UAV LiDAR System

\$ 29,990.99
ONLY

Includes: Rev120 UAV LiDAR System, Subscription Software, Basic Mount, and Battery
Not Included: Training, Drone, Cameras, MMS and Shipping